International Journal of Bifurcation and Chaos, Vol. 14, No. 8 (2004) 2667–2687

DYNAMICS FOR DISCRETE-TIME CELLULAR NEURAL NETWORKS*

SHYAN-SHIOU CHEN and CHIH-WEN SHIH†
Department of Applied Mathematics,
National Chiao Tung University,
Hsinchu, Taiwan, R. O. C.
†*wshih@math.nctu.edu.tw*

Received April 21, 2003; Revised July 1, 2003

This presentation investigates the dynamics of discrete-time cellular neural networks (DT-CNN). In contrast to classical neural networks that are mostly gradient-like systems, DT-CNN possesses both complete stability and chaotic behaviors as different parameters are considered. An energy-like function which decreases along orbits of DT-CNN as well as the existence of a globally attracting set are derived. Complete stability can then be concluded, with further analysis on the sets on which the energy function is constant. The formations of saturated stationary patterns for DT-CNN are shown to be analogous to the ones in continuous-time CNN. Thus, DT-CNN shares similar properties with continuous-time CNN. By confirming the existence of snap-back repellers, hence transversal homoclinic orbits, we also conclude that DT-CNN with certain parameters exhibits chaotic dynamics, according to the theorem by Marotto.

Keywords: Cellular neural network; pattern formation; complete stability; homoclinic orbits; snap-back repeller; chaos.

1. Introduction

Cellular neural network (CNN) is a large aggregation of analogue circuits. It was first proposed by Chua and Yang in 1988. A CNN assembly consists of arrays of identical elementary processing units called cells. The cells are only connected to their nearest neighbors. This local connectivity makes CNN very suitable for VLSI implementation. The equations for a two-dimension layout of CNN are given by

$$C\,\frac{dx_{ij}(t)}{dt} = -\frac{1}{R}x_{ij}(t) + \sum_{(k,\ell)\in N_r(i,j)} [a_{ij,k\ell}h(x_{k\ell}(t)) + b_{ij,k\ell}u_{k\ell}] + I\,, \tag{1}$$

where x_{ij}, $y_{ij} = h(x_{ij})$ are the state and output voltage of the specified CNN cell at site (i, j), respectively; $u_{k\ell}$ is the controlling input. $N_r(i, j)$ represents the neighborhood of (i, j) with radius r (a positive integer). CNN are characterized by the bias I, the template sets A and B which consist of real numbers $a_{ij,k\ell}$ and $b_{ij,k\ell}$, respectively. $a_{ij,k\ell}$ represents the linear feedback, $b_{ij,k\ell}$ the linear control. The standard output function h is a piecewise-linear mapping defined by $h(\xi) = (1/2)(|\xi+1|-|\xi-1|)$. C is the linear capacitor and R is the linear resistor. R and C are often set to $R = 1$ and $C = 1$, for convenience of discussion. A complete set of the CNN model requires imposing boundary condition for the cells on the boundary of the assembly, see [Shih,

*This work is partially supported by the National Science Council, and National Center of Theoretical Sciences of R. O. C. on Taiwan.
†Author for correspondence.

2000]. This presentation will not take into account the boundary conditions, since the approach and methodology used herein prevail even with consideration of boundary conditions. Equation (1) is a continuous-time model, we thus call it CT-CNN.

In this investigation, we shall study the discrete-time cellular neural network (DT-CNN). DT-CNN admits rich dynamics including properties analogous to the ones in CT-CNN. The model is described by the following difference equation.

$$x_{ij}(t+1) = \mu x_{ij}(t) + \sum_{(k,\ell)\in N_r(i,j)} [\tilde{a}_{ij,k\ell} h(x_{k\ell}(t)) + \tilde{b}_{ij,k\ell} u_{k\ell}] + I_{ij}\,, \tag{2}$$

where t is an integer and $(i,\ j)$ belongs to a $n_1 \times n_2$ lattice. Equation (2) can be derived from a delta-operator based CNN. If one collects from a continuous-time signal $\mathbf{x}(t)$ a discrete-time sequence $\mathbf{x}[k] = \mathbf{x}(kT)$, the delta operator

$$\delta\mathbf{x}[k] = \frac{\mathbf{x}[k+1] - \mathbf{x}[k]}{T}$$

is an approximation of the derivative of $\mathbf{x}(t)$. Indeed, $\lim_{T\to 0} \delta\mathbf{x}[k] = \dot{\mathbf{x}}(t)|_{t=kT}$. In this case, $\mu = 1 - T/\tau$, where T is the sampling period, and $\tau = RC$. The parameters $\tilde{a}_{ij,k\ell}, \tilde{b}_{ij,k\ell}$ in (2) correspond to $a_{ij,k\ell}$, $b_{ij,k\ell}$ in (1) under sampling, see [Hänggi *et al.*, 1999]. If (2) is considered in conjunction with (1), then T is required to satisfy $\tau \geq T$ to avoid aliasing effects. Under this situation, $0 \leq \mu \leq 1$ and CT-CNN is the limiting case of delta-operator based CNN with $T \to 0$. If the delta-operator based CNN is considered by itself, then there is no restriction on T, and thus no restrictions on μ in (2). On the other hand, a sample-data based CNN has been introduced in [Harrer & Nossek, 1992]. Such a network corresponds to the limiting case of delta-operator based CNN as $T \to 1$. The readers are referred to [Hänggi *et al.*, 1999] and the reference therein for an account of unifying results on the above-mentioned models. On the other hand, Euler's difference scheme for (1) takes the form

$$x_{ij}(t+1) = \left(1 - \frac{\Delta t}{RC}\right) x_{ij}(t) + \frac{\Delta t}{C}\left(\sum_{k\in N_r(i,j)} a_{ij,k\ell} h(x_{k\ell}(t)) + b_{ij,k\ell} u_{k\ell} + I\right). \tag{3}$$

The parameters in (2) and (3) are related by $\mu = 1 - (\Delta t/RC)$, $\tilde{a}_{ij,k\ell} = (\Delta t/C) a_{ij,k\ell}$, $\tilde{b}_{ij,k\ell} = (\Delta t/C) b_{ij,k\ell}$ and $I_{ij} = (\Delta t/C) I$.

A lattice of any dimension with finitely many sites can be reindexed into a one-dimensional manner. Thus, CNN of any dimension can be reformulated into a one-dimensional setting, cf. [Shih & Weng, 2002]. Restated, the DT-CNN (2) in a two-dimensional layout can be written into a one-dimensional form as

$$x_i(t+1) = \mu x_i(t) + \sum_{k=1}^{n} \omega_{ik} h(x_k(t)) + z_i\,, \tag{4}$$

where $i = 1, \ldots, n$, $n = n_1 \cdot n_2$, and ω_{ik}, z_i correspond to $\tilde{a}_{ij,k\ell}$ and $(\tilde{b}_{ij,k\ell} u_{k\ell} + I_{ij})$, respectively. This expression suppresses local connectivity among cells of DT-CNN. However, it is more concise for our presentation. We shall study DT-CNN in the form (4) for most of this presentation. In the discussions of pattern formation in the last section, the expression of DT-CNN exhibiting local connectivity [such as (2)] will be adopted.

This presentation aims to explore dynamical features of the DT-CNN, including complete stability, chaotic behaviors and pattern formation. By complete stability, we mean that every orbit tends to a steady state solution (fixed point of the DT-CNN herein) as time tends to infinity. Complete stability for the CT-CNN has been studied in [Chua & Yang, 1988; Lin & Shih, 1999; Shih, 2001]. The basic assumption for such a result is the symmetry of the coupling weights, that is, $W := [\omega_{ik}]$ is a symmetric matrix. The situation is much more complicated in DT-CNN. We first derive the existence of a trapping region, and a Lyapunov function V. Because of the saturation part of the output function h, there is a large portion of phase space on which V is constant. We then analyze the dynamics on these regions and conclude complete stability for the DT-CNN, under an additional assumption. We shall also illustrate that formations of saturated stationary solutions and patterns for DT-CNN are analogous to the ones in CT-CNN.

The second goal of this work is to study the snap-back repellers of the DT-CNN. A fixed point $\overline{\mathbf{x}}$ of a map F is said to be a *snap-back repeller* of F if there exists a positive real number r and a point $\mathbf{x}_0 \in B(\overline{\mathbf{x}}; r)$ with $\mathbf{x}_0 \neq \overline{\mathbf{x}}$ such that all eigenvalues of $DF(\mathbf{x})$ exceed unity in norm for all $\mathbf{x} \in B(\overline{\mathbf{x}}; r)$ and $F^m(\mathbf{x}_0) = \overline{\mathbf{x}}$ with $\det(DF^m(\mathbf{x}_0)) \neq 0$ for some positive integer m. Such $\mathbf{x}_0$ is called a *snap-back point*. It is obvious that the existence of snap-back repeller implies the existence of a transversal homoclinic orbit. In 1975, Li and Yorke [1975] proved that period three implies chaos as well as certain sensitive dependence on initial conditions for one-dimensional mappings. It was extended into multidimensional maps by Marotto [1978].

Theorem 1.1 (Marotto). *If F has a snap-back repeller, then the dynamical system $\mathbf{x} \to F(\mathbf{x})$ is chaotic in the following sense*:

(1) There exists a positive integer m_0 such that F has p-periodic points for every integer $p \geq m_0$.
(2) There exists a scrambled set, that is, an uncountable set L containing no periodic points such that the following pertains:
   (a) $F(L) \subset L$;
   (b) for every $\mathbf{y} \in L$ and any periodic point $\mathbf{x}$ of F, $\limsup_{k\to\infty} \|F^k(\mathbf{y}) - F^k(\mathbf{x})\| > 0$;
   (c) for every $\mathbf{x}, \mathbf{y} \in L$ with $\mathbf{x} \neq \mathbf{y}$, $\limsup_{k\to\infty} \|F^k(\mathbf{y}) - F^k(\mathbf{x})\| > 0$.
(3) There exists a uncountable subset L_0 of L such that for every $\mathbf{x}, \mathbf{y} \in L_0$,

$$\liminf_{k\to\infty} \|F^k(\mathbf{y}) - F^k(\mathbf{x})\| = 0\,.$$

Marotto concluded that snap-back repellers imply chaos in the sense of the above theorem. The snap-back repeller, which is suitable for the noninvertible map with repelling fixed points, is a powerful technique for proving chaos in multidimensional maps. Guckenheimer and Holmes [1983] showed that if a diffeomorphism has a transversal homoclinic orbit to the hyperbolic fixed point $\overline{\mathbf{x}}$, then F is locally topologically equivalent to a subshift of finite type. This theorem only applies to diffeomorphisms. Marotto [1979] also applied his theorem to study the transversal homoclinic orbits for the Hénon map.

Classical continuous-time neural networks do not exhibit chaotic behaviors. It is certainly not the case for discrete-time neural networks, see for example, [Chen & Shih, 2002] on a study of the so-called transiently chaotic neural network. Recently, Sbitnev and Chua have studied the local activity criteria and its application to nonhomogeneous spatiotemporal patterns for the DT-CNN. Other mathematical studies in CT-CNN include investigations of pattern formations and spatial entropy, in [Juang & Lin, 2000; Shih, 1998, 2000], and traveling wave solutions [Hsu & Lin, 2000].

In Sec. 2, we shall address the dynamics and demonstrate complete stability and chaotic behaviors of DT-CNN. Rigorous justifications as well as numerical illustrations for these dynamics are presented in Sec. 3. In Sec. 4, we briefly show that formations of saturated stationary patterns for the DT-CNN can be established as in CT-CNN.

2. Dynamics of the DT-CNN

In Sec. 2.1, we shall study the existence of a Lyapunov function, and complete stability for DT-CNN. Chaotic behaviors in the sense of existence of snap-back repellers (hence transversal homoclinic orbits) will be illustrated in Sec. 2.2. We shall illustrate these dynamics numerically in Sec. 3.3.

Let us first discuss the existence of fixed points and their classifications. The following notations are similar to the ones in CT-CNN, see [Lin & Shih, 1999]. First, we partition $\mathbb{R}$ into three regions, according to the configuration of the piecewise linear output function h. Let $\Omega^{\rm l} = \{x \in \mathbb{R} | x \leq -1\}$, $\Omega^{\rm m} = \{x \in \mathbb{R} | -1 < x < 1\}$, $\Omega^{\rm r} = \{x \in \mathbb{R} | x \geq 1\}$. Herein, "l", "m" and "r" mean respectively "left", "middle" and "right". Then $\mathbb{R} = \Omega^{\rm l} \cup \Omega^{\rm m} \cup \Omega^{\rm r}$. Accordingly, we partition $\mathbb{R}^n$ into 3^n regions: $\Omega_{\alpha_1 \cdots \alpha_n} := \{(x_1, \ldots, x_n) \in \mathbb{R}^n | x_1 \in \Omega^{\alpha_1}, \ldots, x_n \in \Omega^{\alpha_n},\ \alpha_i =$ "l", "m", "r"$\}$. Notably, $\Omega_{\rm l} = \Omega^{\rm l}$, $\Omega_{\rm m} = \Omega^{\rm m}$, $\Omega_{\rm r} = \Omega^{\rm r}$, in the case $n = 1$.

Let $\mathcal{D}_{\rm ex} = \{(\alpha_1, \ldots, \alpha_n) | \alpha_i =$ "l" or "r" for all $i = 1, \ldots, n\}$, $\mathcal{D}_{\rm mix} = \{(\alpha_1, \ldots, \alpha_n) | \alpha_i =$ "l" or "r" or "m", and $\alpha_j =$ "m" for at least one $j\}$. We write $\alpha = (\alpha_1, \ldots, \alpha_n)$. Ω_α is called an *exterior region* if $\alpha \in \mathcal{D}_{\rm ex}$, a *mixed region* if $\alpha \in \mathcal{D}_{\rm mix}$, an *interior region* if $\alpha_i =$ "m" for all $i = 1, \ldots, n$. We say that a fixed point $\overline{\mathbf{x}} = (\overline{x}_1, \ldots, \overline{x}_n)$ of (4) is *saturated* if it lies in an exterior region (that is, $|\overline{x}_i| \geq 1$ for every i), *interior* if it lies in the interior region ($|\overline{x}_i| < 1$ for every i) and *mixed* if it lies in a mixed region.

For a fixed point $\overline{\mathbf{x}}$ to exist in an exterior region Ω_α, $\alpha \in \mathcal{D}_{\rm ex}$, it is required that for every

$i = 1, \ldots, n$,

$$\overline{x}_i = \mu \overline{x}_i + \sum_{k=1}^{n} \omega_{ik} \delta_k + z_i \,,$$

with $\overline{x}_i \geq 1$ if $\alpha_i =$ "r", and $\overline{x}_i \leq -1$ if $\alpha_i =$ "l". Herein, $\delta_k = -1$, if $\alpha_k =$ "l" and $\delta_k = 1$, if $\alpha_k =$ "r". Hence, the fixed point in each exterior region, if exists, is unique.

For a fixed point $\overline{\mathbf{x}}$ to exist in the interior region Ω_α, $\alpha = (\mathrm{m}, \ldots, \mathrm{m})$, the following equations have to be satisfied for $\mathbf{x} = \overline{\mathbf{x}}$

$$x_i = \mu x_i + \sum_{k=1}^{n} \omega_{ik} x_k + z_i \,, \tag{5}$$

and $|\overline{x}_i| < 1$ for all $i = 1, \ldots, n$.

Consider a mixed region Ω_α, $\alpha = (\alpha_1, \ldots, \alpha_n) \in \mathcal{D}_{\mathrm{mix}}$. Let $J_0 = \{i | \alpha_i =$ "m"$\}$ and $J_1 = \{i | \alpha_i =$ "l", "r"$\}$. For a fixed point $\overline{\mathbf{x}}$ to exist in the mixed region, the following system of linear equations needs to be satisfied for $\mathbf{x} = \overline{\mathbf{x}}$:

$$x_i - \mu x_i - \sum_{k \in J_0} \omega_{ik} x_k = \sum_{k \in J_1} \omega_{ik} \delta_k + z_i \,, \tag{6}$$

for $i \in J_0$ and $|\overline{x}_i| < 1$, and for $i \in J_1$

$$\overline{x}_i := \frac{1}{1-\mu} \left[\sum_{k \in J_1} \omega_{ik} \delta_k + \sum_{k \in J_0} \omega_{ik} \overline{x}_k + z_i \right] \tag{7}$$

satisfies $\overline{x}_i \geq 1$ if $\alpha_i =$ "r", $\overline{x}_i \leq -1$ if $\alpha_i =$ "l". Herein, again, $\delta_k = -1$, if $\alpha_k =$ "l" and $\delta_k = 1$, if $\alpha_k =$ "r". Therefore, it is possible that the fixed points in the mixed regions or the interior region appear as a continuum. Since (5) and (6) are linear systems, one can easily derive conditions on the parameters so that each of these linear systems has a unique solution. We shall call these parameters *regular*. Thus, for the DT-CNN with regular parameters, if a fixed point exists in a region Ω_α, then it is unique and isolated. Notably, there may exist semi-invariant subsets in a mixed region Ω_α, $\alpha = (\alpha_1, \ldots, \alpha_n) \in \mathcal{D}_{\mathrm{mix}}$. Indeed, if $\overline{\mathbf{x}}$ satisfies (6), let

$$I_\alpha := \{\mathbf{x} = (x_1, \ldots, x_n) | x_i = \overline{x}_i \ \text{ if } i \in J_0 \,, \\ x_i \geq 1 \ \text{ if } \alpha_i = \text{"r"}, x_i \leq -1 \ \text{ if } \alpha_i = \text{"l"}\} \,. \tag{8}$$

For a point $\mathbf{x}$ in this set $I_\alpha \subset \Omega_\alpha$, forward iterations of $\mathbf{x}$ under (4) stay in I_α, before entering another region $\Omega_{\alpha'}$, as (4) is respected.

2.1. *Complete stability*

Let us denote the n-dimensional map in (4) by

$$F_i(\mathbf{x}) = \mu x_i + \sum_{k=1}^{n} \omega_{ik} h(x_k) + z_i \,, \tag{9}$$

where $i = 1, \ldots, n$. Notably, $F = (F_1, \ldots, F_n)$ restricted to each region Ω_α is an affine map. The domain of this map can be extended to $\mathbb{R}^n$, and we denote this extended map by F_{Ω_α}. By *complete stability*, we mean that every solution of the system tends to a stationary solution as time goes to positive infinity. Such a property is also called convergence of dynamics, cf. [Fiedler & Gedeon, 1998; Shih & Weng, 2000]. To conclude such a property, one needs to assure first that every solution is bounded.

Proposition 2.1. *If $0 < \mu < 1$, then there exists a globally attracting set for (9).*

Proof. Assume $0 < \mu < 1$. Let

$$M = \frac{1}{1-\mu} \left[\max_{i=1,\ldots,n} \left(\sum_{k=1}^{n} |\omega_{ik}| + |z_i| \right) \right] .$$

Then, $\mu x_i - (1-\mu)M \leq F_i(\mathbf{x}) \leq \mu x_i + (1-\mu)M$ for every i. Hence, if $\mathbf{x} = (x_1, \ldots, x_n) \in \mathbb{R}^n$ with $|x_i| \leq M$ for every i, then $|F_i(\mathbf{x})| \leq M$. It follows that the set $\mathcal{A} = \{(x_1, \ldots, x_n) \in \mathbb{R}^n | -M \leq x_i \leq M\}$ is a positively invariant set. On the other hand, let $\mathbf{x} = (x_1, \ldots, x_n) \in \mathbb{R}^n$ with $|x_i| > M$ for every i. We only need to consider each component of F. Let $x_i > M$, then

$$\begin{aligned} x_i &> \mu x_i + \sum_{k=1}^{n} |\omega_{ik}| + |z_i| \\ &\geq \left| \mu x_i + \sum_{k=1}^{n} \omega_{ik} h(x_k) + z_i \right| \\ &= |F_i(\mathbf{x})| \,. \end{aligned}$$

On the other hand, for $x_i < -M$, we have

$$x_i < -\frac{1}{1-\mu} \left(\sum_{k=1}^{n} |\omega_{ik}| + |z_i| \right) ,$$

and then

$$\begin{aligned} x_i &< \mu x_i - \sum_{k=1}^{n} |\omega_{ik}| - |z_i| \\ &\leq - \left| \mu x_i + \sum_{k=1}^{n} \omega_{ik} h(x_k) + z_i \right| \\ &= -|F_i(\mathbf{x})| \,. \end{aligned}$$

We have shown that $|F_i(\mathbf{x})| < |x_i|$ for all $\mathbf{x} = (x_1, \ldots, x_n)$ with $|x_i| > M$ for all i. Accordingly, it can be justified that $\mathcal{A}$ is a globally attracting set for (9). ■

Let us introduce the following Lyapunov function for DT-CNN:

$$V(\mathbf{x}) = -\frac{1}{2}\sum_{i=1}^{n}\sum_{k=1}^{n}\omega_{ik}h(x_i)h(x_k) - \sum_{i=1}^{n} z_i h(x_i) + \frac{1}{2}(1-\mu)\sum_{i=1}^{n} h(x_i)^2\,, \quad (10)$$

where $h(\xi) = (1/2)(|\xi + 1| - |\xi - 1|)$ and $\mathbf{x} = (x_1, \ldots, x_n) \in \mathbb{R}^n$. It will be shown in Sec. 3 that

$$V(F(\mathbf{x})) - V(\mathbf{x}) \leq -\frac{1}{2}(\Delta\mathbf{y})^T W(\Delta\mathbf{y})\,,$$

where $\Delta\mathbf{y} = (\Delta y_1, \ldots, \Delta y_n)$ and $\Delta y_i = h(F_i(\mathbf{x})) - h(x_i)$, $i = 1, \ldots, n$, under the assumptions that $0 \leq \mu \leq 1$, and the matrix of connection weights $W = [\omega_{ik}]$ is symmetric. We thus obtain the following proposition.

Proposition 2.2. *Let $W = [\omega_{ik}]$ be a positive-definite symmetric matrix and $0 \leq \mu \leq 1$. Then $V(F(\mathbf{x})) - V(\mathbf{x}) \leq 0$, for all $\mathbf{x} \in \mathbb{R}^n$.*

The proof will be given in Sec. 3. Notably, since $h(\xi) = 1$ for $\xi \geq 1$ and $h(\xi) = -1$ for $\xi \leq -1$, V is constant on every exterior region. In addition, V is constant on every segment $\tilde{I}$ of a mixed region Ω_α, $\alpha = (\alpha_1, \ldots, \alpha_n) \in \mathcal{D}_{\text{mix}}$, where $\tilde{I}$ is of the form

$$\{\mathbf{x} \in \Omega_\alpha | x_i \geq 1 \ \text{ if } \alpha_i = \text{“r”},\ x_i \leq -1 \ \text{ if } \alpha_i = \text{“l”},\ x_i = \xi_i \ \text{ if } \alpha_i = \text{“m”}\}\,,$$

where $-1 < \xi_i < 1$ is an arbitrary number. Concerning the asymptotic behaviors of (9), we should then study the dynamics on the set on which V is constant, according to the LaSalle's invariant principle (quoted in Sec. 3.1). Figure 1 illustrates a typical graph of function V for the case $n = 2$.

Let $S_0 = \{\mathbf{x} \in \mathbb{R}^n | V(F(\mathbf{x})) - V(\mathbf{x}) = 0\}$. Notably, by the definition of S_0 and the computations in the proof of Proposition 2.2, $\mathbf{x} \in S_0$ if and only if $h(F_i(\mathbf{x})) = h(x_i)$, for all $i = 1, \ldots, n$. For each i, the equation $h(F_i(\mathbf{x})) = h(x_i)$ holds for the following three cases, due to the definition of the piecewise linear output function h: (a) $F_i(\mathbf{x}) = x_i$, (b) $F_i(\mathbf{x}) \geq 1$ and $x_i \geq 1$, (c) $F_i(\mathbf{x}) \leq -1$ and $x_i \leq -1$.

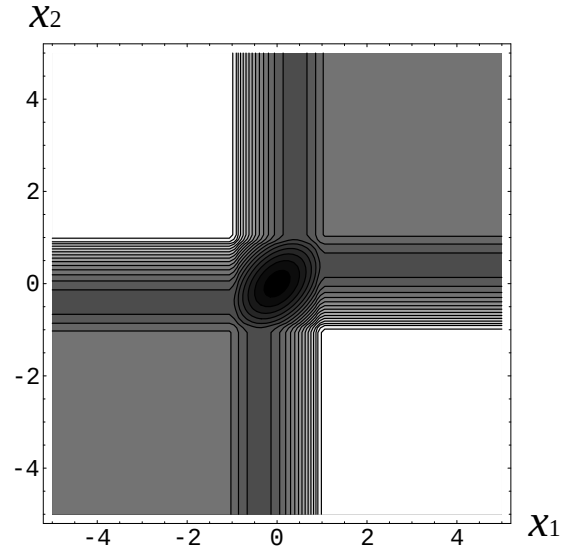

(a)

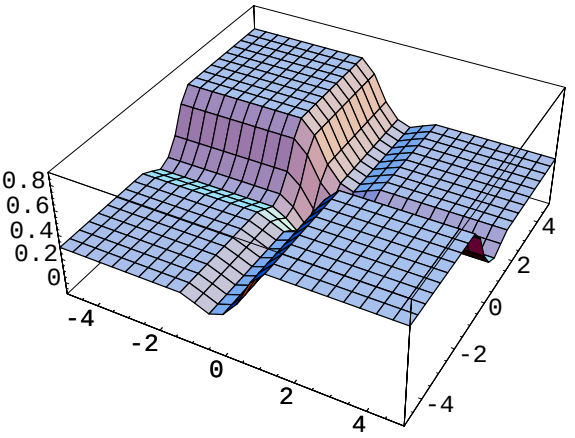

(b)

Fig. 1. $V(\mathbf{x})$ is constant on exterior regions and some segments of mixed regions for DT-CNN with $n = 2, \mu = 0.2$, $\omega = 0.3$, $\omega_{12} = \omega_{21} = 0.2$, $z_2 = z_1 = 0$. (a) The contour plots for function V. (b) The graph of function V.

Thus, S_0 is contained in the union S of the following sets:

$$\{\mathbf{x} \in \Omega_\alpha | -1 < x_i = F_i(\mathbf{x}) < 1 \ \text{ if } \alpha_i = \text{“m”}\,,\ x_i \geq 1 \ \text{ if } \alpha_i = \text{“r”}\,,\ x_i \leq -1 \ \text{ if } \alpha_i = \text{“l”}\}\,.$$

Restated,

$$S := \left(\bigcup_{\alpha\in\mathcal{D}_{\text{ex}}} \Omega_\alpha\right) \cup \left(\bigcup_{\alpha\in\mathcal{D}_{\text{mix}}} I_\alpha\right) \cup \mathcal{E}_0\,, \quad (11)$$

where $\mathcal{E}_0$ is the set of fixed points in the interior region, and I_α is defined in (8). We shall call each of the sets Ω_α, I_α, $\mathcal{E}_0$ in (10) a *component* of S.

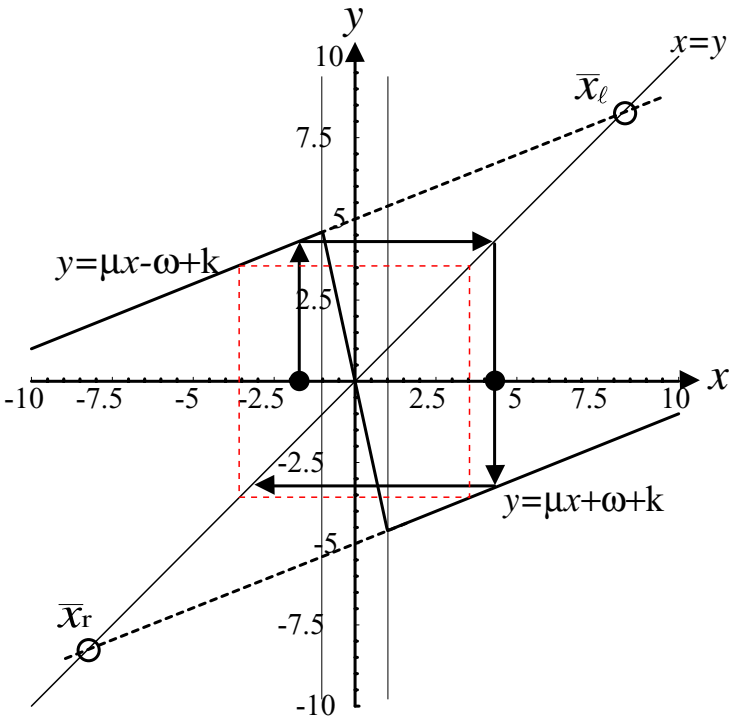

Fig. 2. The graph of $f(x) = \mu x + \omega h(x) + k$ with the parameter $\mu = 0.4$, $\omega = -5$ and $k = 0$. (DPS) fails to hold. In fact, there exists an attracting periodic orbit with period 2.

Notably, these components of S are pairwise disjoint if (9) with regular parameters are considered.

We say that a point $\overline{\mathbf{x}}$ is a *virtual fixed point* of (9) if it is a fixed point for the affine map F_{Ω_α} associated with the restriction of F to Ω_α, but fails to lie in Ω_α. For example, take (9) with $n = 2$, $\mu = 0.2$, $\omega = 0.5$, $\omega_{12} = \omega_{21} = 0.2$ and $z_1 = z_2 = 0$. Then $I_{\rm rm} = \{(x_1, x_2) | x_1 > 1,\ x_2 = 2/3\}$ and the fixed point $(19/24, 2/3)$ is a virtual fixed point of $F_{\Omega_{\rm rm}}$. Indeed, this fixed point does not belong to $\Omega_{\rm rm}$.

Here, we shall denote that Ω_α, $\alpha = (\alpha_1, \ldots, \alpha_n)$, is *more interior* than $\Omega_{\alpha'}$, $\alpha' = (\alpha'_1, \ldots, \alpha'_n)$, if $\alpha_i =$ "m" and $\alpha'_i =$ "r" or "l" for some i and $\alpha_i = \alpha'_i$ for all other i.

By the LaSalle's invariant principle, the ω-limit set of every orbit lies in S_0. The following two properties for the dynamics of (9) on S are needed to get control on the iterations of points in $S_0 \subset S$, and then to conclude complete stability for the DT-CNN.

(CPS) – a convergent property on components of S: If there is a stable fixed point $\overline{\mathbf{x}}$ in a component of S, then $\overline{\mathbf{x}}$ attracts every point in this component.

(DPS) – a divergent property on components of S: If there is no stable fixed point in a component ($\subseteq \Omega_\alpha$ for some α) of S, then every orbit starting in the component leaves the component and enters into a region which is more interior than Ω_α, in finite forward iterates.

In contrast to the situation in CT-CNN [Lin & Shih, 1999], additional conditions need to be imposed to guarantee these two properties for DT-CNN. It is straightforward to see from (9) that (CPS) holds if $0 < \mu < 1$. On the other hand, Fig. 2 gives an illustration for the situation that (DPS) does not hold for (9) with $n = 1$. In Fig. 2, $\overline{x}_{\rm l}$ is a virtual fixed point of $F_{\Omega_{\rm l}}$, and $\overline{x}_{\rm r}$ is a virtual fixed point of $F_{\Omega_{\rm r}}$. Points in $\Omega_{\rm l}$ are iterated into $\Omega_{\rm r}$ which is not more interior than $\Omega_{\rm l}$. But, to conclude complete stability, we require that forward iterations of points in $\Omega_{\rm r}$ (resp. $\Omega_{\rm l}$) can only lie in $\Omega_{\rm m} \cup \Omega_{\rm r}$ (resp. $\Omega_{\rm m} \cup \Omega_{\rm l}$). With the following condition (H), the virtual fixed points $\overline{x}_{\rm r}$ of $F_{\Omega_{\rm r}}$ and $\overline{x}_{\rm l}$ of $F_{\Omega_{\rm l}}$ satisfy $\overline{x}_{\rm r} > -1$ and $\overline{x}_{\rm l} < 1$. Under the circumstances, the situation like Fig. 2 does not occur.

The conditions for the existence of fixed points and virtual fixed points of (9) are very complicated. Herein, we get around with this complication by formulating an assumption which takes into account the possibility of existence of semi-invariant subset I_α in every mixed region Ω_α. We recall that a fixed point of (9) in a mixed region Ω_α lies in I_α, and

forward iterations of points in I_α under (9) stay in I_α, before entering another region $\Omega_{\alpha'}$.

Let us introduce the following notations $\delta(\alpha_i, \alpha_k)$ and $z(i)$:

$$\delta(\alpha_i, \alpha_k) = \begin{cases} 1\,, & \text{if } \alpha_i = \alpha_k \\ -1\,, & \text{if } \alpha_i \neq \alpha_k\,, \end{cases}$$

where $\alpha_i, \alpha_k =$ "l" or "r";

$$z(i) = \begin{cases} -z_i\,, & \text{if } \alpha_i = \text{"l"} \\ z_i\,, & \text{if } \alpha_i = \text{"r"}\,. \end{cases}$$

We consider the following additional condition: for $i = 1, \ldots, n$, with $\alpha_i =$ "r" or "l",

$$\text{(H)} \quad \frac{1}{1-\mu}\left[\omega_{ii} - \sum_{k,\alpha_k=\text{"m"}} |\omega_{ik}| + \sum_{k\neq i,\alpha_k\neq\text{"m"}} \delta(\alpha_i,\alpha_k)\omega_{ik} + z(i)\right] > -1\,.$$

Consequently, if $\overline{\mathbf{x}} = (\overline{x}_1, \ldots, \overline{x}_n)$ is a virtual fixed point of F_{Ω_α}, $\alpha \in \mathcal{D}_{\text{mix}}$ or $\mathcal{D}_{\text{ex}}$, then $\overline{x}_i > -1$ (resp. $\overline{x}_i < 1$) if $\alpha_i =$ "r" (resp. $\alpha_i =$ "l"). Under the assumption (H) and $0 < \mu < 1$, if $\alpha_i =$ "r" (resp. $\alpha_i =$ "l"), then $x_i \geq F_i(\mathbf{x}) > -1$ (resp. $x_i \leq F_i(\mathbf{x}) < 1$), for all $\mathbf{x} \in I_\alpha$ if $\alpha \in \mathcal{D}_{\text{mix}}$ and for all $\mathbf{x} \in \Omega_\alpha$ if $\alpha \in \mathcal{D}_{\text{ex}}$. Thus, (H) and $0 < \mu < 1$ ensure that forward iterations of points in a component of S without a fixed point enter into more interior regions, that is, (DPS) holds. Notably, if the parameters of DT-CNN are regular, then there are at most 3^n components for S and the component $\mathcal{E}_0$ in the interior region only consists of the fixed point of F.

According to the LaSalle's invariant principle, Propositions 2.1, 2.2 and the above arguments, we can conclude the following theorem on complete stability for the DT-CNN. Detailed proof for the theorem is given in Sec. 3.1.

Theorem 2.3. *Let W be a positive-definite symmetric matrix. If $0 < \mu < 1$ and the condition* (H) *holds, then the DT-CNN with regular parameters is completely stable.*

Remark. Theorem 2.3 can be generalized from symmetric W to cycle-symmetric ones, via a suitable change of coordinates, as in [Shih, 2001].

2.2. *Illustrations of chaotic dynamics*

In this section, we shall illustrate the construction of homoclinic orbits and snap-back repellers for the two-cell DT-CNN system, that is, (4) or (9) with $n = 2$. The existence of snap-back repellers results in chaotic dynamics of DT-CNN, according to Marotto's theorem. Notably, F is an affine mapping when restricted to each of the nine regions $\Omega_{\star *}$, $\star, * =$ "l", "m", "r". For simplicity, we take $\omega = \omega_{11} = \omega_{22}$, $z_1 = z_2 = z$. Equation (9) with $n = 2$ becomes:

$$F_1(x_1, x_2) = \mu x_1 + \omega h(x_1) + \omega_{12} h(x_2) + z\,, \quad (12)$$

$$F_2(x_1, x_2) = \mu x_2 + \omega h(x_2) + \omega_{21} h(x_1) + z\,. \quad (13)$$

To find fixed points of the system, we need to solve $F_1(x_1, x_2) = x_1$, $F_2(x_1, x_2) = x_2$. For example, if we look for a fixed point in the middle region Ω_{mm}, then the following equation (F restricted to Ω_{mm}) should be considered.

$$\mu x_1 + \omega h(x_1) + \omega_{12} h(x_2) + z = \mu x_1 + \omega x_1 + \omega_{12} x_2 + z = x_1\,, \quad (14)$$

$$\mu x_2 + \omega h(x_2) + \omega_{21} h(x_1) + z = \mu x_2 + \omega x_2 + \omega_{21} x_1 + z = x_2\,. \quad (15)$$

Under suitable parameter conditions, one can find solution (x_1, x_2) of (14), (15) with $|x_1|, |x_2| < 1$. We denote this fixed point in Ω_{mm} by $(\overline{x}_1, \overline{x}_2)$. Fixed points in other regions can be found similarly.

Next, to construct a homoclinic orbit, we shall find pre-images of the fixed point $(\overline{x}_1, \overline{x}_2)$. To this end, the equation $F(x_1, x_2) = (\overline{x}_1, \overline{x}_2)$ needs to be solved, that is,

$$\mu x_1 + \omega h(x_1) + \omega_{12} h(x_2) + z = \overline{x}_1\,, \quad (16)$$

$$\mu x_2 + \omega h(x_2) + \omega_{21} h(x_1) + z = \overline{x}_2\,. \quad (17)$$

If we aim at finding the first pre-image of $(\overline{x}_1, \overline{x}_2)$ in Ω_{ll}, we should consider (16), (17) restricted to Ω_{ll}. In this case, with $h(x_1) = h(x_2) = -1$, we obtain the solution $x_1 = (1/\mu)(\overline{x}_1 + \omega + \omega_{12} - z)$ and $x_2 = (1/\mu)(\overline{x}_2 + \omega + \omega_{21} - z)$. If these two values are less than minus one, then (x_1, x_2) is indeed a pre-image of $(\overline{x}_1, \overline{x}_2)$, which is located in Ω_{ll}. If so, we denote this point (x_1, x_2) by $(\overline{x}_1^{-1,\text{l}}, \overline{x}_2^{-1,\text{l}})$, which reads as the first pre-image of $(\overline{x}_1, \overline{x}_2)$ lying in Ω_{ll}. Finding a further pre-image of $(\overline{x}_1, \overline{x}_2)$ amounts to finding the pre-image of $(\overline{x}_1^{-1,\text{l}}, \overline{x}_2^{-1,\text{l}})$. That is, we solve for (x_1, x_2) in the following system:

$$\mu x_1 + \omega h(x_1) + \omega_{12} h(x_2) + z = \overline{x}_1^{-1,\text{l}}$$

$$\mu x_2 + \omega h(x_2) + \omega_{21} h(x_1) + z = \overline{x}_2^{-1,\text{l}}.$$

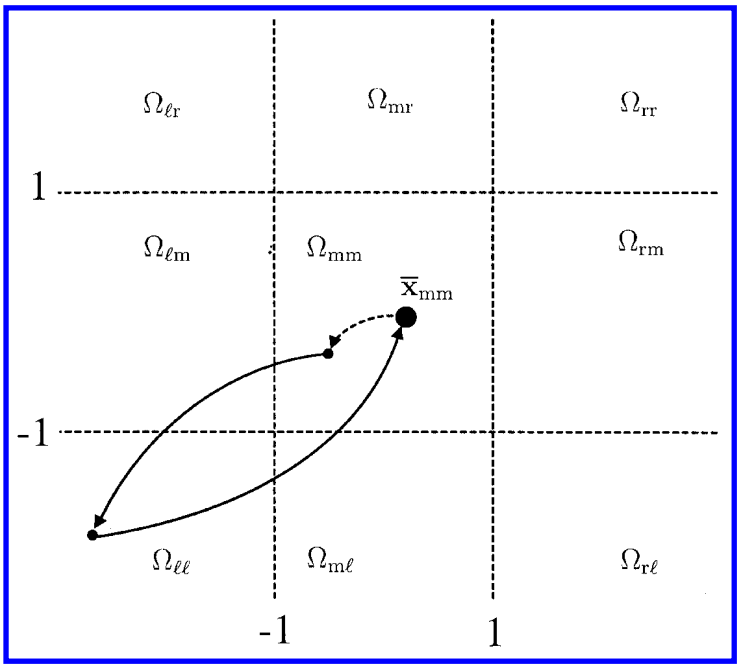

Fig. 3. The big dot denotes the snap-back repeller $\overline{\mathbf{x}}_{mm} = (\overline{x}_1, \overline{x}_2)$ of F in Ω_{mm}. The other small dots are successive pre-images of $\overline{\mathbf{x}}_{mm}$ under F. The graph shows that there exists a homoclinic orbit for $\overline{\mathbf{x}}_{mm}$.

Table 1. Numerical values for a backward orbit of the fixed point (0, 0), for DT-CNN with $n = 2$, $\mu = -1.5$, $\omega = 50$, $\omega_{12} = 0.4$ and $\omega_{21} = -0.4$. This orbit is a homoclinic orbit for DT-CNN.

$(\overline{x}_1, \overline{x}_2)$	$= (0, 0)$
$(\overline{x}_1^{-1,l}, \overline{x}_2^{-1,l})$	$= (-33.6, -33.0667)$
$(\overline{x}_1^{-2,m}, \overline{x}_2^{-2,m})$	$= (-0.687114, -0.687454)$
$(\overline{x}_1^{-3,m}, \overline{x}_2^{-3,m})$	$= (-1.40494 * 10^{-2}, -1.42902 * 10^{-2})$
$(\overline{x}_1^{-4,m}, \overline{x}_2^{-4,m})$	$= (-2.8723 * 10^{-4}, -2.97012 * 10^{-4})$
$\vdots$	$\vdots$
$(\overline{x}_1^{-k,m}, \overline{x}_2^{-k,m})$	$\to (0, 0)$ as $k \to \infty$.

If there exists a solution (x_1, x_2) to this system of equations, which lies in Ω_{mm}, then we shall denote this point by $(\overline{x}_1^{-2,m}, \overline{x}_2^{-2,m})$. One can find successive pre-images of $(\overline{x}_1, \overline{x}_2)$ lying in all possible regions; for example, $\{(\overline{x}_1^{-1,l}, \overline{x}_2^{-1,l})$, $(\overline{x}_1^{-2,m}, \overline{x}_2^{-2,m})$, $(\overline{x}_1^{-3,m}, \overline{x}_2^{-3,m})$, $\ldots\}$, as illustrated in Fig. 3. If F is expanding on Ω_{mm}, and $(\overline{x}_1^{-k,m}, \overline{x}_2^{-k,m}) \to (\overline{x}_1, \overline{x}_2)$, as $k \to \infty$, then this orbit is a homoclinic orbit for (9) with $n = 2$. Table 1 illustrates a numerical computation of such an orbit for (9) with the indicated parameters.

The above-mentioned scheme describes the basic ideas for constructing homoclinic orbits for DT-CNN. However, technical difficulties arise in locating the parameters to guarantee the existence of solutions for the associated linear systems and suitable magnitudes of the components for these solutions. We shall propose an approach which combines using the structure of the one-dimensional DT-CNN with the standard Brouwer's fixed point theorem for the constructions of homoclinic orbits.

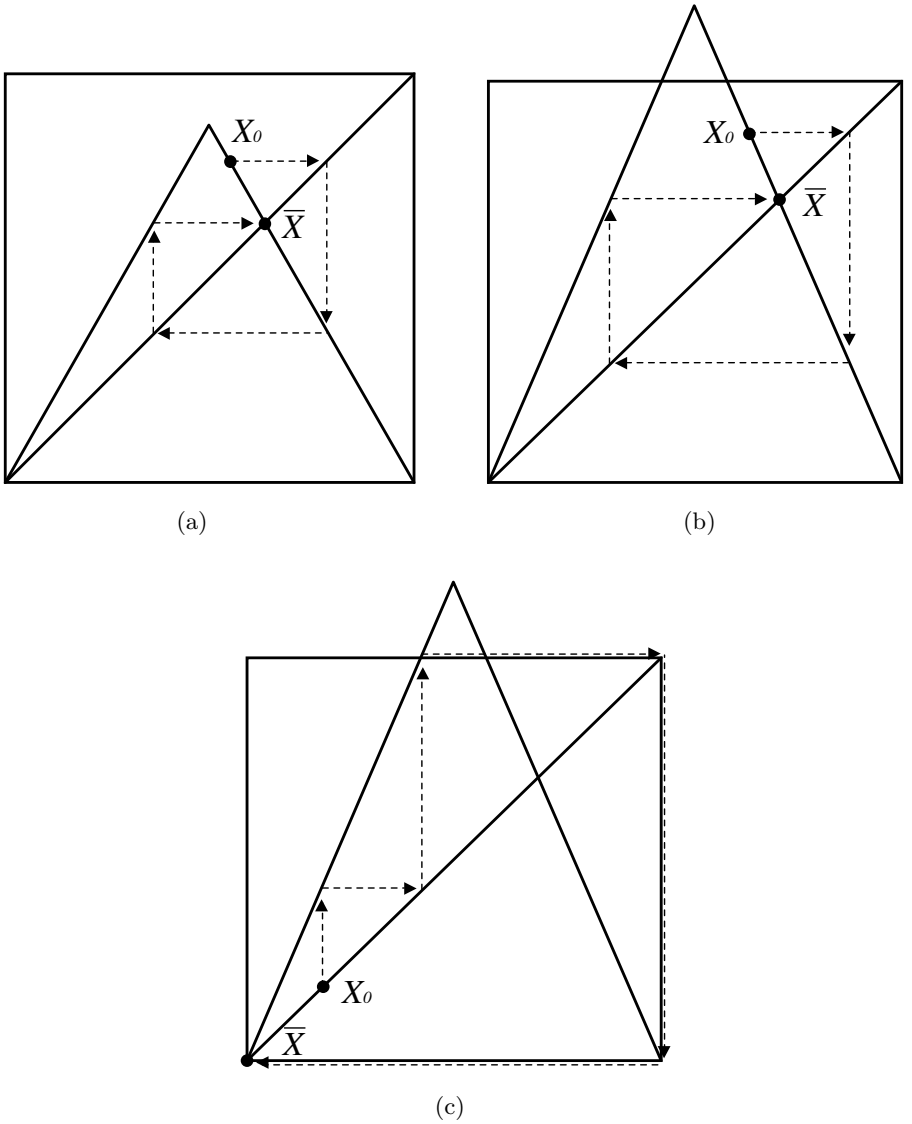

Fig. 4. In (a)–(c), successive pre-images for fixed point $\overline{\mathbf{x}}$ can be found so that some points in the backward orbit of $\overline{\mathbf{x}}$ lie in a neighborhood of $\overline{\mathbf{x}}$. Thus, $\overline{\mathbf{x}}$ is a snap-back repeller with snap-back point $\mathbf{x}_0$.

We plan to sketch our approach in this section and arrange the details in Sec. 3.2. First, let us consider three tent maps with slope $\pm s$, $s > 1$. In each graph of Fig. 4, it is easily observed that there exists a homoclinic orbit through $\overline{\mathbf{x}}$, and $\mathbf{x}_0$ is a snap-back point. Thus, $\overline{\mathbf{x}}$ is a snap-back repeller, by the definition of snap-back repeller.

Let us consider the case of a single-cell DT-CNN, $f(x) = \mu x + \omega h(x) + \kappa$ with $h(x) = (1/2)(|x+1| - |x-1|)$. Under some parameter conditions, the graph of f is as Fig. 5. It can be seen that each of the shaded regions in Fig. 5 is like a tent map in Figs. 4(b) and 4(c). Though the lower-left shaded region of Fig. 5 is upside-down, finding pre-images for the repelling fixed point is similar to the situation in Figs. 4(b) and 4(c). Hence, we can easily trace the backward orbit for each of the three fixed points of f in Fig. 5. We remark that instead of solving the associated linear systems to find the pre-images of fixed points, we adopt a geometric approach herein. Restated, we explore suitable configurations for the graph of f to meet our purpose. Such a treatment allows us to formulate the conditions on the parameters to conclude the desired results. For example, since μ and $\mu + \omega$ are the slopes of f, the conditions $\mu < -1$, $\mu + \omega > 1$, and $|\kappa/(\mu + \omega - 1)| < 1$ imply that there exist three repelling fixed points and that the middle fixed point $\kappa/(\mu + \omega - 1)$ belongs to Ω^{m}.

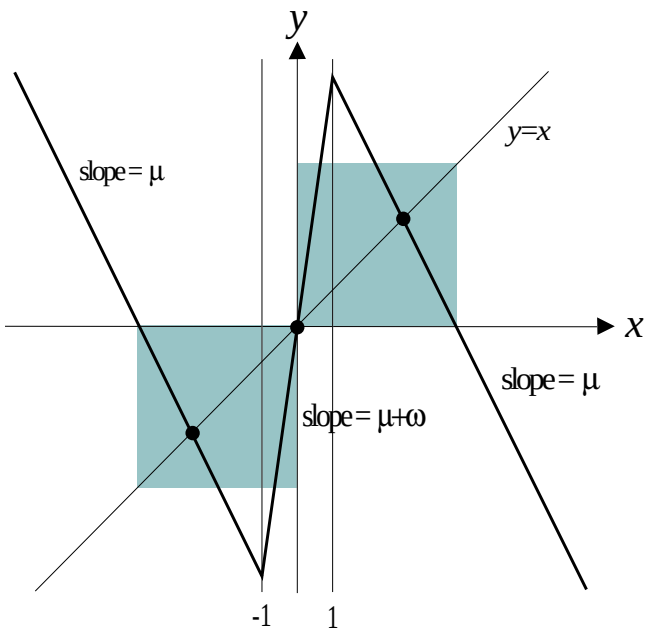

Fig. 5. The configuration for one-dimensional DT-CNN.

To extend the scenario of Fig. 5 to multidimensional DT-CNN, we need to establish a family of one-dimensional maps which have similar configurations as Fig. 5. Consider the two-cell DT-CNN (12), (13). Since $|h| \leq 1$, we have

$$\check{f}(x_1) \leq F_1(x_1, x_2) \leq \hat{f}(x_1)\,, \tag{18}$$

$$\check{f}(x_2) \leq F_2(x_1, x_2) \leq \hat{f}(x_2)\,, \tag{19}$$

where $\hat{f}(\xi) = \mu\xi + \omega h(\xi) + \kappa$ and $\check{f}(\xi) = \mu\xi + \omega h(\xi) - \kappa$, and $\kappa := \max\{|\omega_{12}| + |z|, |\omega_{21}| + |z|\}$. For any $\rho_1, \rho_2 \in \mathbb{R}$ and $\xi \in \mathbb{R}$, if we take $f_{\rho_2}(\xi) = F_1(\xi, \rho_2)$ or $f_{\rho_1}(\xi) = F_2(\rho_1, \xi)$, then $\check{f}(\xi) \leq f_{\rho_i}(\xi) \leq \hat{f}(\xi)$, $i = 1, 2$, by (18), (19). Under certain parameter conditions, the configurations for $\hat{f}$, $\check{f}$, and the family $\{f_{\rho_i}\}$ are as illustrated in Fig. 6(a).

Let $(\overline{x}_1, \overline{x}_2)$ be a fixed point of (12), (13). For each $(\rho_1, \rho_2) \in \Omega_{\star *}$, $\star, * =$ "r", "m", "l", we consider the equations

$$\mu x_1 + \omega h(x_1) + \omega_{12} h(\rho_2) + z = \overline{x}_1\,, \tag{20}$$

$$\mu x_2 + \omega h(x_2) + \omega_{21} h(\rho_1) + z = \overline{x}_2\,. \tag{21}$$

Solving (20) for x_1 (resp. (21) for x_2) can be regarded as solving the equation $f_{\rho_2}(\xi) = \overline{x}_1$ (resp. $f_{\rho_1}(\xi) = \overline{x}_2$) for ξ. Assume that the configuration in Fig. 6(b) holds. It follows that for η in certain range, we can always find $-1 < \xi_i' < 1$ and $\xi_i'' > 1$ such that $f_{\rho_2}(\xi_1') = f_{\rho_2}(\xi_1'') = \eta$ and

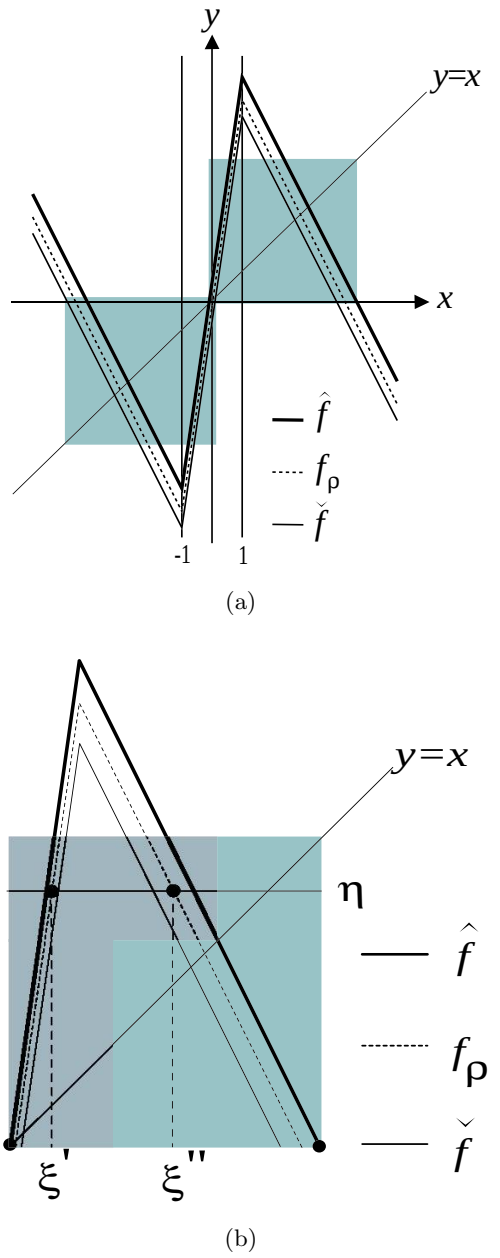

Fig. 6. The graph of a family of single-cell maps f_ρ. There exist three fixed points for each f_ρ. Each fixed point is a snap-back repeller. (a) The scenario for a family of maps $\{f_\rho\}$, whose members differ by vertical shifts. (b) Blow-up of the right-upper region of (a), $f_\rho(\xi') = f_\rho(\xi'') = \eta$.

$f_{\rho_1}(\xi_2') = f_{\rho_1}(\xi_2'') = \eta$. Herein, $\overline{x}_1$ or $\overline{x}_2$ are regarded as η in Fig. 6(b). The scenario confirms the existence of solutions $(x_1, x_2) = (\xi_1', \xi_2')$, (ξ_1', ξ_2''), (ξ_1'', ξ_2'), (ξ_1'', ξ_2'') for (18), (19). We regard the correspondence $(\rho_1, \rho_2) \mapsto (\xi_1', \xi_2')$ or (ξ_1', ξ_2'') or (ξ_1'', ξ_2') or (ξ_1'', ξ_2'') as a mapping $G : \Omega_{**} \to \Omega_{**}$, where $\star, * =$ "m", "r". Similar discussions hold for the lower-left part of Fig. 6(a). A fixed point of G gives a preimage of $(\overline{x}_1, \overline{x}_2)$. Obviously, a unique fixed point

in $\Omega_{\star *}$ exists if G is a contraction mapping on $\Omega_{\star *}$. Thus we shall impose conditions so that the scenario in Fig. 6(a) holds and G is a continuous mapping on each region $\Omega_{\star *}$. To find further pre-images of $(\overline{x}_1, \overline{x}_2)$, we again consider (20), (21) with $(\overline{x}_1, \overline{x}_2)$ replaced by the first pre-image of $(\overline{x}_1, \overline{x}_2)$.

To guarantee that each fixed point is a repeller, we require that F is expanding on each of the nine regions $\Omega_{\star *}$, $\star, * =$ "l", "m", "r". This property holds if we require $\mu + \omega > 1 + \kappa$. Indeed, let us take the region $\Omega_{\rm mm}$ for an illustration. F on $\Omega_{\rm mm}$ is a linear system with coefficient matrix

$$L = \begin{pmatrix} \mu + \omega - 1 & \omega_{12} \\ \omega_{21} & \mu + \omega - 1 \end{pmatrix}.$$

The magnitudes for the eigenvalues of L are greater than one, under the condition $\mu + \omega > 1 + \kappa$, by the Gerschgorin's theorem.

3. Verifications for the Dynamics of DT-CNN

3.1. *Complete stability*

In this section, we shall provide rigorous proof for the dynamics of DT-CNN. We plan to justify the complete stability and the existence of snap-back repellers for DT-CNN in Secs. 3.1 and 3.2, respectively. Several numerical illustrations are arranged in Sec. 3.3.

Proof of Proposition 2.2. Recall V defined in (9),

$$V(\mathbf{x}) = -\frac{1}{2}\sum_{i=1}^{n}\sum_{k=1}^{n}\omega_{ik}h(x_i)h(x_k) - \sum_{i=1}^{n} z_i h(x_i) + \frac{1}{2}(1-\mu)\sum_{i=1}^{n} h(x_i)^2 .$$

It follows that

$$V(F(\mathbf{x})) - V(\mathbf{x}) = -\frac{1}{2}\sum_{i=1}^{n}\sum_{k=1}^{n}\omega_{ik}h(F_i(\mathbf{x}))h(F_k(\mathbf{x})) - \sum_{i=1}^{n} z_i h(F_i(\mathbf{x})) + \frac{1}{2}(1-\mu)\sum_{i=1}^{n} h(F_i(\mathbf{x}))^2$$
$$- \left[-\frac{1}{2}\sum_{i=1}^{n}\sum_{k=1}^{n}\omega_{ik}h(x_i)h(x_k) - \sum_{i=1}^{n} z_i h(x_i) + \frac{1}{2}(1-\mu)\sum_{i=1}^{n} h(x_i)^2\right]. \tag{22}$$

Let $\Delta y_i = h(F_i(\mathbf{x})) - h(x_i)$. We substitute $z_i = -\mu x_i - \sum_{k=1}^{n}\omega_{ik}h(x_k) + F_i(\mathbf{x})$, by (9). Equation (22) becomes

$$-\frac{1}{2}\sum_{i=1}^{n}\sum_{k=1}^{n}\omega_{ik}\Delta y_i\Delta y_k - \frac{1}{2}\sum_{i=1}^{n}\sum_{k=1}^{n}\omega_{ik}[h(x_i)\Delta y_k + h(x_k)\Delta y_i]$$
$$+\sum_{i=1}^{n}\left(\mu x_i + \sum_{k=1}^{n}\omega_{ik}h(x_k) - F_i(\mathbf{x})\right)\Delta y_i + \frac{1}{2}(1-\mu)\sum_{i=1}^{n}[h(F_i(\mathbf{x}))^2 - h(x_i)^2]$$
$$= -\frac{1}{2}\sum_{i=1}^{n}\sum_{k=1}^{n}\omega_{ik}\Delta y_i\Delta y_k - \mu\sum_{i=1}^{n}[F_i(\mathbf{x}) - x_i]\Delta y_i + \sum_{i=1}^{n}(\mu-1)F_i(\mathbf{x})\Delta y_i$$
$$+\frac{1}{2}(1-\mu)\sum_{i=1}^{n}[h(F_i(\mathbf{x}))^2 - h(x_i)^2]$$
$$= -\frac{1}{2}\sum_{i=1}^{n}\sum_{k=1}^{n}\omega_{ik}\Delta y_i\Delta y_k - \mu\sum_{i=1}^{n}[F_i(\mathbf{x}) - x_i]\Delta y_i$$
$$-(1-\mu)\sum_{i=1}^{n}\left(F_i(\mathbf{x})\Delta y_i - \frac{1}{2}[h(F_i(\mathbf{x}))^2 - h(x_i)^2]\right). \tag{23}$$

In the above computations, the first equality follows from the symmetry of $W = [w_{ik}]$. Let $\Gamma_i(\mathbf{x}) = F_i(\mathbf{x})\Delta y_i - (1/2)[h(F_i(\mathbf{x}))^2 - h(x_i)^2]$ in (23), for $i = 1, \ldots, n$. We divide the following discussions into three cases.

(i) $|F_i(\mathbf{x})| < 1$: $\Gamma_i(\mathbf{x}) = F_i(\mathbf{x})\Delta y_i - F_i(\mathbf{x})\Delta y_i + (1/2)(\Delta y_i)^2 = (1/2)(\Delta y_i)^2 \geq 0$.

(ii) $F_i(\mathbf{x}) \geq 1$:

(a) $x_i \geq 1$: $\Gamma_i(\mathbf{x}) = F_i(\mathbf{x})(1-1) - (1/2)(1^2 - 1^2) = 0$;

(b) $|x_i| \leq 1$:

$$\begin{aligned}\Gamma_i(\mathbf{x}) &= F_i(\mathbf{x})(1-x_i) - \frac{1}{2}[1^2 - (x_i)^2] \\ &\geq 1 - x_i - \frac{1}{2} + \frac{1}{2}(x_i)^2 \\ &= \frac{1}{2}(x_i - 1)^2 \geq 0\,;\end{aligned}$$

(c) $x_i \leq -1$: $\Gamma_i(\mathbf{x}) = F_i(\mathbf{x})[1-(-1)] - (1/2)[1^2 - (-1)^2] = 2F_i(\mathbf{x}) \geq 2$.

(iii) $F_i(\mathbf{x}) \leq -1$:

(a) $x_i \geq 1$: $\Gamma_i(\mathbf{x}) = F_i(\mathbf{x})[-1-1] - (1/2)[(-1)^2 - 1^2] = -2F_i(\mathbf{x}) \geq 2$;

(b) $|x_i| \leq 1$:

$$\begin{aligned}\Gamma_i(\mathbf{x}) &= F_i(\mathbf{x})[-1-x_i] - \frac{1}{2}[(-1)^2 - (x_i)^2] \\ &\geq 1 + x_i - \frac{1}{2} + \frac{1}{2}(x_i)^2 \\ &= \frac{1}{2}(x_i + 1)^2 \geq 0\,;\end{aligned}$$

(c) $x_i \leq -1$: $\Gamma_i(\mathbf{x}) = F_i(\mathbf{x})[-1-(-1)] - (1/2)[(-1)^2 - (-1)^2] = 0$.

By (i)–(iii), $\Gamma_i \geq 0$ for all i. $[F_i(\mathbf{x}) - x_i][h(F_i(\mathbf{x})) - h(x_i)] \geq 0$, since h is non-decreasing. Therefore, if $0 \leq \mu \leq 1$, (23) is no larger than $-(1/2)(\Delta\mathbf{y})^t W \Delta\mathbf{y}$, where $\Delta\mathbf{y} = (\Delta y_1, \ldots, \Delta y_n)$. Since W is positive-definite, $V(F(\mathbf{x})) \leq V(\mathbf{x})$ for all $\mathbf{x} \in \mathbb{R}^n$. This completes the proof. ■

Let us recall the LaSalle's invariant principle for difference equations:

$$\mathbf{x}(t+1) = F(\mathbf{x}(t))\,, \tag{24}$$

where F: $\mathbb{R}^n \to \mathbb{R}^n$ is a continuous function. Let U be a subset of $\mathbb{R}^n$. For a function V: $U \to \mathbb{R}$, define $\dot{V}(\mathbf{x}) = V(F(\mathbf{x})) - V(\mathbf{x})$. V is said to be a *Lyapunov function* of (24) on U if (i) V is continuous, and (ii) $\dot{V}(\mathbf{x}) \leq 0$ for all $\mathbf{x} \in U$. Set

$$S_0 = \{\mathbf{x} \in \overline{U} | \dot{V}(\mathbf{x}) = 0\}\,.$$

LaSalle's Invariant Principle [LaSalle, 1976]. *Let F be a continuous mapping on $\mathbb{R}^n$, and let V be a Lyapunov function for F on a set $U \subseteq \mathbb{R}^n$. If $\gamma : \{F^k(\mathbf{x}) | k \in \mathbb{N}\}$, the positive orbit of a point $\mathbf{x}$, is contained in a compact set and $\gamma \subset U$, then its ω-limit set $\omega(\gamma) \subset S_0 \cap V^{-1}(c)$ for some $c = c(\mathbf{x})$.*

We shall apply the LaSalle's invariant principle in the following proof of Theorem 2.3.

Proof of Theorem 2.3. It follows from $0 < \mu < 1$ and the assumption (H) that (CPS) and (DPS) hold. Consider the positive orbit $\gamma : \{F^k(\mathbf{x}) | k \in \mathbb{N}\}$ of an arbitrary point $\mathbf{x}$. Denote by $\omega(\gamma)$, the ω-limit set of γ, which is bounded and invariant. It follows from Proposition 2.1 that there exists a globally attracting set for (9). Note that this globally attracting set is a compact set. Accordingly, any positive orbit γ will be contained in a compact set. In addition, with W being symmetric and positive-definite, V is a Lyapunov function for (9) on $\mathbb{R}^n$, by Proposition 2.2. Hence, $\omega(\gamma)$ is contained in S_0, due to the LaSalle's invariant principle. Suppose $\overline{\mathbf{x}} \in \omega(\gamma)$ and $\overline{\mathbf{x}}$ is not a fixed point of F, then $F^k(\overline{\mathbf{x}})$ belongs to $\omega(\gamma)$ for any integer $k \in \mathbb{N}$, according to the definition of $\omega(\gamma)$. Moreover, $V(F^k(\overline{\mathbf{x}})) = V(\overline{\mathbf{x}})$. If $F^k(\overline{\mathbf{x}})$ enters into a region which is not in S_0, then V decreases. So, $F^k(\overline{\mathbf{x}})$ has to remain in S_0 for any $k \in \mathbb{N}$. Therefore, $F^k(\overline{\mathbf{x}})$ travels among components of S_0 and these components are pairwise disjoint under the assumption that the parameters for DT-CNN are regular. Assume that $\overline{\mathbf{x}}$ belongs to an exterior region Ω_α. If there is a fixed point in Ω_α, then it must be stable and attracts all points in Ω_α, due to (CPS). In this case, $\overline{\mathbf{x}}$ has to be this fixed point. If there is no fixed point in Ω_α, then forward iterations of $\overline{\mathbf{x}}$ enter into a component of S in region $\Omega_{\alpha'}$ which is more interior than Ω_α, due to (DPS). If this component is $\mathcal{E}_0$, then since $\mathcal{E}_0$ only consists of a stable fixed point of F under the assumption of the theorem, a contradiction to $\overline{\mathbf{x}} \in \omega(\gamma)$ arises. If this component is $I_{\alpha'}$ in a mixed region $\Omega_{\alpha'}$, then similar arguments indicate that either there is a contradiction to $\overline{\mathbf{x}} \in \omega(\gamma)$ or further iterations of $\overline{\mathbf{x}}$ enter a region which is more interior than $\Omega_{\alpha'}$, due to (CPS) and (DPS). Since there are at most 3^n components for S, the situation that forward iterations of $\overline{\mathbf{x}}$ eventually enter into $\mathcal{E}_0$ in the interior region $\Omega_{\mathrm{m}\cdots\mathrm{m}}$ again yields a contradiction. If $\overline{\mathbf{x}}$ lies in I_α of some mixed region, then similar arguments yield a contradiction. We conclude that if $\overline{\mathbf{x}} \in \omega(\gamma)$, then $\overline{\mathbf{x}}$ is a fixed point of F. In addition, it follows from Lemma 2.7 of [Hale & Raugel, 1992] that $\omega(\gamma)$ is connected. Thus $\omega(\gamma)$ consists of only one fixed point. This completes the proof. ■

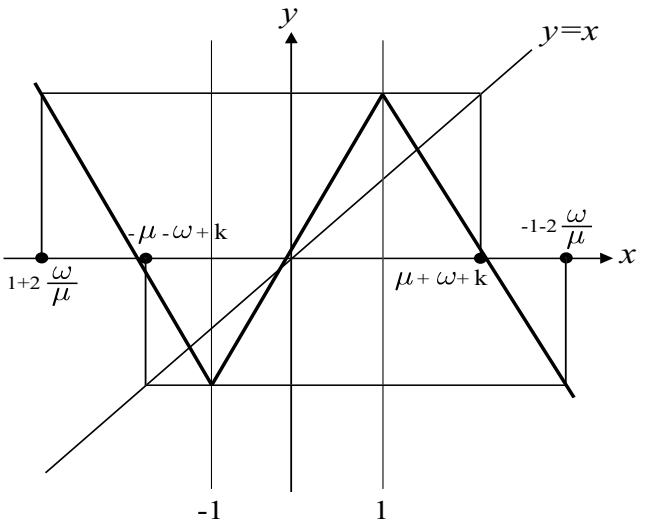

(a)

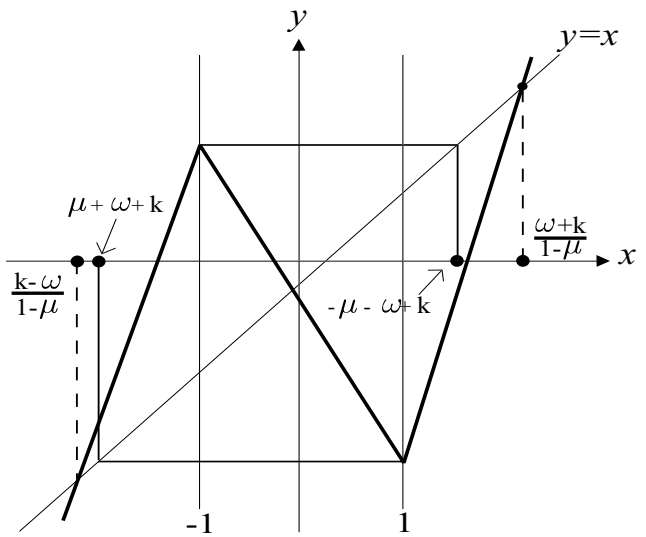

(b)

Fig. 7. Configurations for the one-dimensional DT-CNN. (a) The parameters satisfy Proposition 3.1(i). (b) The parameters satisfy Proposition 3.1(ii).

3.2. *Chaotic behaviors*

3.2.1. *One-dimensional DT-CNN*

Let f: $\mathbb{R} \to \mathbb{R}$ be the single-cell DT-CNN which takes the following form:

$$f(x) = \mu x + \omega h(x) + \kappa\,, \tag{25}$$

where $h(x) = (1/2)(|x+1| - |x-1|)$. A compact region K is called a *trapping region* for f provided $f(K) \subset \text{int}(K)$. We shall show that there exists a trapping region for f satisfying some parameter conditions. Existence of trapping regions assures that iterations of the system do not diverge to infinity.

Note that the point $\kappa/(\mu+\omega-1)$ is a fixed point of (25) if $|\kappa/(\mu+\omega-1)| < 1$; moreover, the graph of f has two slopes $\mu+\omega$, μ, and f has three fixed points if $\mu+\omega > 1$, $\mu < -1$ [see Fig. 7(a)], or, $\mu+\omega < -1$, $\mu > 1$ [see Fig. 7(b)]. Furthermore, these fixed points are all repelling.

Proposition 3.1

(i) *Assume that* $\mu+\omega > 1$, $\mu < -1$, $|\kappa/(\mu+\omega-1)| < 1$ *and* $\mu+\omega+\kappa < -1-2(\omega/\mu)$, $1+2(\omega/\mu) < -\mu-\omega+\kappa$, *then there exists a trapping region containing* $[-\mu-\omega+\kappa, \mu+\omega+\kappa]$ *for the single-cell DT-CNN.*

(ii) *Assume that* $\mu+\omega < -1$, $\mu > 1$, $|\kappa/(\mu+\omega-1)| < 1$ *and* $(\omega+\kappa)/(1-\mu) > -\mu-\omega+\kappa$, $\mu+\omega+\kappa > (\kappa-\omega)/(1-\mu)$, *then there exists a trapping region containing* $[\mu+\omega+\kappa, -\mu-\omega+\kappa]$ *for the single-cell DT-CNN.*

Let us explain the main idea of Proposition 3.1 by some figures. In Fig. 7(a) corresponding to case (i), the graph of f is like a reverse N-shape figure. The local minimum and local maximum occur at -1 and 1, respectively. The forward iterations of the local minimum $-\mu-\omega+\kappa$ and local maximum $\mu+\omega+\kappa$, under f, are all between the first pre-images of the minimum and the maximum, $-1-2(\omega/\mu)$ and $1+2(\omega/\mu)$, marked in Fig. 7(a). Figure 7(b) corresponds to case (ii). Both the local minimum $\mu+\omega+\kappa$, and the local maximum $-\mu-\omega+\kappa$, are between the two fixed points $(\kappa-\omega)/(1-\mu)$, $(\omega+\kappa)/(1-\mu)$. The assertions thus follow.

The following formulations will be used to prove the existence of snap-back repellers for the multidimensional DT-CNN. For $\kappa > 0$, $|\rho| \le \kappa$, let

$$\hat{f}(x) = \mu x + \omega h(x) + \kappa\,,$$
$$\check{f}(x) = \mu x + \omega h(x) - \kappa\,,$$
$$f_\rho(x) = \mu x + \omega h(x) + \rho\,.$$

It is obvious that $\check{f} \le f_\rho \le \hat{f}$ due to $|\rho| \le \kappa$. We call $\hat{f}$ the *upper-map* and $\check{f}$ the *lower-map*. These two piecewise linear functions $\hat{f}$ and $\check{f}$ are drawn in Fig. 8(a), and f_ρ is between $\hat{f}$ and $\check{f}$.

We classify the parameter conditions for the existence of fixed points, snap-back repellers, as well as trapping regions as follows:

(PC-1-a) $\mu+\omega > 1+\kappa$, $\mu < -1-\kappa$, $|\kappa/(\mu+\omega-1)| < 1$

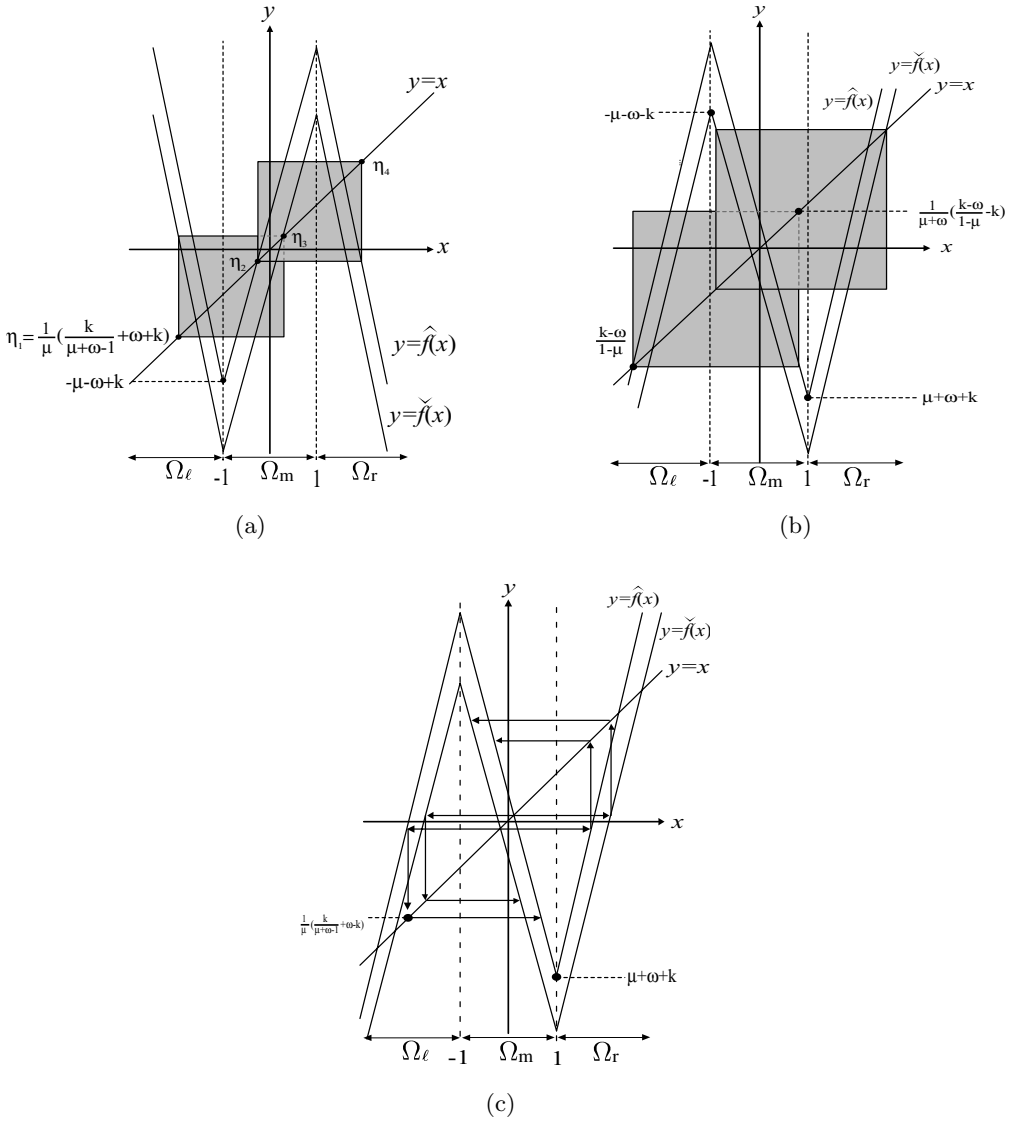

Fig. 8. Configurations for the upper and lower maps $\hat{f}$ and $\check{f}$ which satisfy conditions in Proposition 3.2. The parameters satisfy (a), (b) condition (i), (c) condition (ii), of Proposition 3.2.

(PC-1-b) $(1/\mu)[(\kappa/(\mu+\omega-1))+\omega+\kappa] > -\mu-\omega+\kappa$

(PC-1-c) $\mu+\omega+\kappa < -1-2(\omega/\mu)+2(\kappa/\mu)$

(PC-2-a) $\mu+\omega < -1-\kappa$, $\mu > 1+\kappa$, $|\kappa/(\mu+\omega-1)| < 1$

(PC-2-b(i)) $(1/(\mu+\omega))[(\kappa-\omega)/(1-\mu) - \kappa] < -\mu-\omega-\kappa$

(PC-2-b(ii)) $(1/\mu)[\kappa/(\mu+\omega-1)+\omega-\kappa] > \mu+\omega+\kappa$

(PC-2-c) $(\omega+\kappa)/(1-\mu) > -\mu-\omega+\kappa$.

(PC-1-a), (PC-2-a) are related to existence of three fixed points; (PC-1-b), (PC-2-b) are associated with existence of snap-back repellers; (PC-1-c), (PC-2-c) correspond to the trapping regions, for the DT-CNN. Notably, in (PC-1-b), $\kappa/(\mu+\omega-1)$ is the middle fixed point of $\check{f}$ and $[\kappa/(\mu+\omega-1)+\omega+\kappa]/\mu$ is the left pre-image of this value $\kappa/(\mu+\omega-1)$ under $\check{f}$. Condition (PC-1-b) means that this pre-image value is larger than $\hat{f}(-1)$, cf. Fig. 8(a). By symmetry for the graphs of $\check{f}$ and $\hat{f}$, imposing this condition on the left-handed part of the configuration for $\check{f}$ and $\hat{f}$ yields the same effect to the right-handed part. In addition, conditions (PC-1-a) and (PC-1-c) with $\kappa > 0$ imply the condition in Proposition 3.1(i). Similar situations hold for the other conditions in (PC-2) and Proposition 3.1(ii).

Proposition 3.2. *Let $\kappa > 0$ and $\check{f} \le f_\rho \le \hat{f}$ be defined as above.*

(i) *If* (PC-1-a,-b) *or* (PC-2-a,-b(i)) *hold, then there exist three snap-back repellers for the map* f_ρ.
(ii) *If* (PC-2-a,-b(ii)) *hold, then there exists at least one snap-back repeller which lies in the middle region* $\Omega_{\rm m}$ *for the map* f_ρ.

Proposition 3.2 can be seen from the following observations. In Fig. 8(a), if $\eta \in [\eta_1, \eta_3]$, then there exist two pre-images $\eta^{-1,{\rm l}}$ and $\eta^{-1,{\rm m}}$ of η under f_ρ lying in $\Omega_{\rm l}$ and $\Omega_{\rm m}$, respectively, due to (PC-1-b). Similarly, if $\eta \in [\eta_2, \eta_4]$ and (PC-1-b) holds, then there exist two pre-images $\eta^{-1,{\rm m}}$ and $\eta^{-1,{\rm r}}$ of η under f_ρ lying in $\Omega_{\rm m}$ and $\Omega_{\rm r}$, respectively. Consider the middle fixed point $\overline{x}$ of f_ρ lying in $\Omega_{\rm m}$. It then lies in $[\eta_1, \eta_3]$ obviously. We choose the pre-image $\overline{x}^{-1,{\rm l}} \in \Omega_{\rm l}$ of $\overline{x}$. Since $\overline{x}^{-1,{\rm l}}$ belongs to the interval $[\eta_1, \eta_3]$, there exists a pre-image $\overline{x}^{-2,{\rm m}}$ of $\overline{x}^{-1,{\rm l}}$, which lies in $\Omega_{\rm m}$. Since the inverse of f_ρ restricted to $\Omega_{\rm m}$ is contracting, one can construct a homoclinic orbit for the fixed point $\overline{x}$ accordingly. With the slope assumption on f_ρ, it can be concluded that $\overline{x}$ is a snap-back repeller. The situations for other cases in Proposition 3.2 are similar.

Remark. There is a difference between items (i) and (ii) in Proposition 3.2, concerning the existence of trapping region. More precisely, there are parameters satisfying condition (ii) of Proposition 3.2 and condition (ii) of Proposition 3.1 simultaneously. It is not the case for condition (i) of Proposition 3.2 and condition (i) of Proposition 3.1.

3.2.2. *Multidimensional DT-CNN*

In the subsection, we shall verify the existence of snap-back repellers for the multidimensional DT-CNN. Rewrite (4) or (8) as

$$F_i(\mathbf{x}) = \mu x_i + \omega h(x_i) + \sum_{k\neq i}^{n} \omega_{ik} h(x_k) + z_i\,, \quad i = 1, \ldots, n\,, \qquad h(\xi) = \frac{1}{2}(|\xi + 1| - |\xi - 1|)\,. \tag{26}$$

First, we consider the trapping region of (26). Our idea is to get control of every component F_i of the multidimensional DT-CNN. Given the map (26), for $i = 1, \ldots, n$, let

$$\kappa_i = \sum_{k\neq i}^{n} |\omega_{ik}| + |z_i|\,, \tag{27}$$

$$\begin{aligned} \check{f}_i(\xi) &= \mu\xi + \omega h(\xi) - \kappa_i\,, \\ \hat{f}_i(\xi) &= \mu\xi + \omega h(\xi) + \kappa_i\,. \end{aligned} \tag{28}$$

Theorem 3.3. *There exists a trapping region for* (*26*)*, which contains*

(I) $T := [-\mu - \omega - \kappa_1, \mu + \omega + \kappa_1] \times \cdots \times [-\mu - \omega - \kappa_n, \mu + \omega + \kappa_n]$, *provided* (PC-1-a,-c) *holds for the parameters* (μ, ω, κ_i), $i = 1, \ldots, n$;
(II) $T := [\mu + \omega - \kappa_1, -\mu - \omega + \kappa_1] \times \cdots \times [\mu + \omega - \kappa_n, -\mu - \omega + \kappa_n]$, *provided* (PC-2-a,-c) *holds for the parameters* (μ, ω, κ_i), $i = 1, \ldots, n$.

Proof. Let us explain case (I) of Theorem 3.3. In Fig. 9(a), $-1 - 2\omega/\mu + 2\kappa_i/\mu$ is the right-handed pre-image of $\hat{f}_i(-1) = -\mu - \omega + \kappa_i$ under $\check{f}_i$, and $1 + 2\omega/\mu - 2\kappa_i/\mu$ is the left-handed pre-image of $\check{f}_i(1) = \mu + \omega - \kappa_i$ under $\hat{f}_i$. Notably, the interval $[1 + 2\omega/\mu - 2\kappa_i/\mu,\ -1 - 2\omega/\mu + 2\kappa_i/\mu]$ contains the interval $[\check{f}_i(-1), \hat{f}_i(1)]$, under conditions (PC-1-a,-c). To justify the assertion, we divide the interval $[-\mu - \omega - \kappa_i, \mu + \omega + \kappa_i]$ into three parts $[-\mu - \omega - \kappa_i, -1]$, $[-1, 1]$ and $[1, \mu + \omega + \kappa_i]$, for each i.

(i) If $x_i \in [-\mu - \omega - \kappa_i, -1]$, we have $-\mu - \omega - \kappa_i = \check{f}_i(-1) \le \check{f}_i(x_i) \le F_i(\mathbf{x}) \le \hat{f}_i(x_i) \le \hat{f}_i(-\mu - \omega - \kappa_i) \le \mu + \omega + \kappa_i$.
(ii) If $x_i \in [1, \mu + \omega + \kappa_i]$, a computation similar to (i) shows that $-\mu - \omega - \kappa_i \le F_i(\mathbf{x}) \le \mu + \omega + \kappa_i$.
(iii) If $x_i \in [-1, 1]$, it follows that $F_i(\mathbf{x}) \in [\check{f}(-1), \hat{f}(1)] = [-\mu - \omega - \kappa_i, \mu + \omega + \kappa_i]$.

Case (II) follows from similar arguments, see Fig. 9(b). ■

Next, let us consider the fixed points for the map (26).

Theorem 3.4. *Let* κ_i *and* $\check{f}_i, \hat{f}_i$ *be defined as* (*27*), (*28*)*. Assume that* (PC-1-a) *or* (PC-2-a) *holds for the parameters* (μ, ω, κ_i), $i = 1, \ldots, n$, *then there exist* 3^n *fixed points of* (*26*) *in* $\mathbb{R}^n$.

Proof. Notably, every component F_i of the map F satisfies $\check{f}_i(x_i) \le F_i(\mathbf{x}) \le \hat{f}_i(x_i)$, for all $\mathbf{x}$. Consider a fixed region Ω_α for certain $\alpha = (\alpha_1, \ldots, \alpha_n)$, $\alpha_i =$ "l", "m" or "r". Let $(\xi_1', \ldots, \xi_n') \in \Omega_\alpha$ be given. Then, under condition (PC-1-a) or (PC-2-a) for each i, there exist $\xi_i^{\rm l} \in \Omega^{\rm l}$, $\xi_i^{\rm m} \in \Omega^{\rm m}$, $\xi_i^{\rm r} \in \Omega^{\rm r}$ such that

$$\xi_i^* = \mu\xi_i^* + \omega h(\xi_i^*) + \sum_{k\neq i}^{n} \omega_{ik} h(\xi_k') + z_i\,, \tag{29}$$

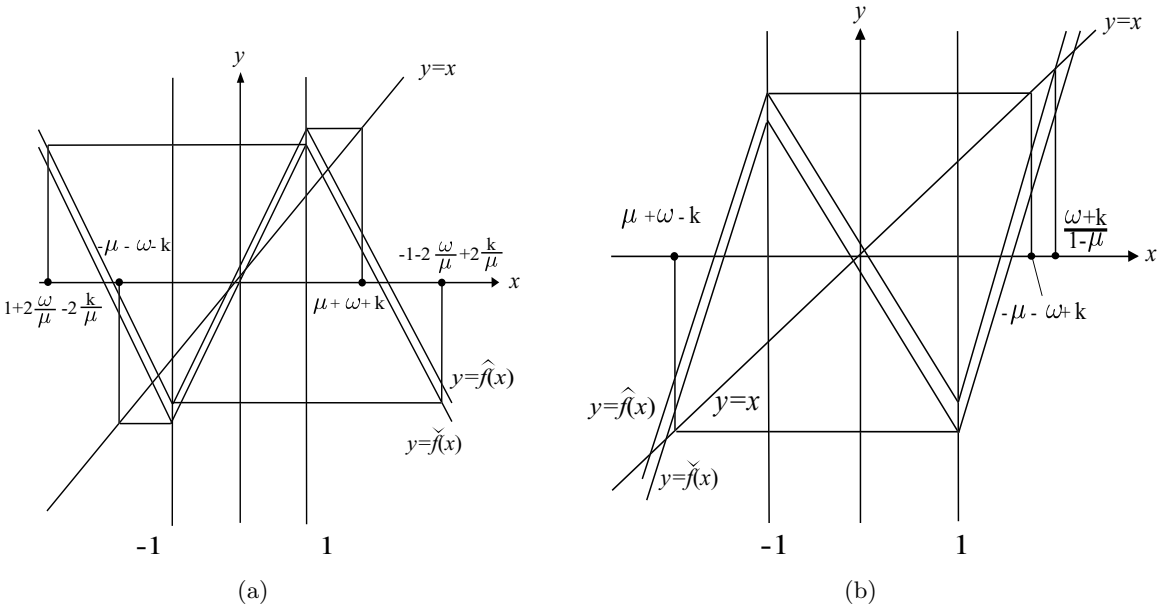

Fig. 9. Configurations for $\check{f}$ and $\hat{f}$ satisfying the conditions in (a) Theorem 3.3 (I), (b) Theorem 3.3 (II).

where "$*$" = "l", "m", "r". Restated, each ξ_i^* is a fixed point of the one-dimensional map $\xi_i \mapsto \mu\xi_i + \omega h(\xi_i) + \sum_{k\neq i}^n \omega_{ik} h(\xi_k') + z_i$. The correspondence gives a map H: $\Omega_\alpha \to \Omega_\alpha$ in the following form:

$$H_i(\xi') = \begin{cases} \dfrac{1}{1-\mu}\left[\displaystyle\sum_{k\neq i}^n \omega_{ik} h(\xi_k') + \omega + z_i\right] & \text{if } \alpha_i = \text{"r"} \\ \dfrac{1}{1-\mu-\omega}\left[\displaystyle\sum_{k\neq i}^n \omega_{ik} h(\xi_k') + z_i\right] & \text{if } \alpha_i = \text{"m"} \\ \dfrac{1}{1-\mu}\left[\displaystyle\sum_{k\neq i}^n \omega_{ik} h(\xi_k') - \omega + z_i\right] & \text{if } \alpha_i = \text{"l"}, \end{cases}$$

where $\xi' = (\xi_1', \ldots, \xi_n')$ and $H = (H_1, \ldots, H_n)$. It is clear that H is a continuous function on Ω_α. Hence, by the Brouwer's fixed point theorem, there exists one fixed point $\overline{\mathbf{x}}$ of H in Ω_α, which is also a fixed point of F. In fact, there exists only one fixed point in each Ω_α, as to be seen in the proof of Theorem 3.5. Consequently, there are 3^n fixed points of F in $\mathbb{R}^n$. ■

The following theorem mainly concerns itself with the existence of the snap-back repeller for (26). The idea is, again, setting up a good control on every component of F first and using the Brouwer's fixed point theorem to obtain suitable pre-images of the fixed point and confirm the existence of homoclinic orbits.

Theorem 3.5. *If* (PC-1-a,-b) *or* (PC-2-a,-b(i)) *holds for the parameters* (μ, ω, κ_i), $i = 1, \ldots, n$, *then there exist* 3^n *snap-back repellers for* (26). *If* (PC-2-a,-b(ii)) *holds, then there exists at least one snap-back repeller of* (26), *which lies in the interior region.*

Proof. We only verify the (PC-1-a,-b) case. Notably, $\mu + \omega > 1 + \kappa_i$, $\mu < -1 - \kappa_i$ and $|\kappa_i/(\mu + \omega - 1)| < 1$ imply the existence of 3^n fixed points of (26), due to Theorem 3.4. Each of the 3^n regions Ω_α, $\alpha_i =$ "l" or "m" or "r", contains exactly one of these fixed points. The proof is divided into three steps (I)–(III).

(I) For each $i = 1, \ldots, n$, there is a scenario as Fig. 8(a), under condition (PC-1-a,-b). That is, if $\eta \in [\eta_1^i, \eta_3^i]$ (resp. $\eta \in [\eta_2^i, \eta_4^i]$), then for any $\xi = (\xi_1, \ldots, \xi_n) \in \mathbb{R}^n$, there exist $\xi_i' \in \Omega^{\mathrm{m}}$, and $\xi_i'' \in \Omega^{\mathrm{l}}$, (resp. $\xi_i' \in \Omega^{\mathrm{m}}$ and $\xi_i'' \in \Omega^{\mathrm{r}}$) such that, for $x_i = \xi_i', \xi_i''$

$$\eta = \mu x_i + \omega h(x_i) + \sum_{k\neq i}^n \omega_{ik} h(\xi_k) + z_i\,.$$

(II) Let $\overline{\mathbf{x}} = (\overline{x}_1, \ldots, \overline{x}_n)$ be a fixed point in Ω_α, $\alpha = (\alpha_1, \ldots, \alpha_n)$, $\alpha_i =$ "l" or "m" or "r". Notice that $\overline{x}_i \in [\eta_1^i, \eta_3^i]$ (resp. $[\eta_2^i, \eta_4^i]$) if $\alpha_i =$ "l" (resp. $\alpha_i =$ "r"), and $\overline{x}_i \in [\eta_1^i, \eta_3^i] \cap [\eta_2^i, \eta_4^i]$ if $\alpha_i =$ "m". Choose $\alpha' = (\alpha_1', \ldots, \alpha_n')$ such that $\alpha_i' =$ "l", or "r", if $\alpha_i =$ m, and $\alpha_i' =$ "m", if $\alpha_i =$ "l" or "r". Let $\xi = (\xi_1, \ldots, \xi_n) \in \Omega_{\alpha'}$,

then there exists $(x_1, \ldots, x_n) \in \Omega_{\alpha'}$, satisfying

$$\overline{x}_i = \mu x_i + \omega h(x_i) + \sum_{k \neq i}^{n} \omega_{ik} h(\xi_k) + z_i\,, \quad i = 1, \ldots, n\,,$$

according to (I). The correspondence defines the following map $\overline{H} : \Omega_{\alpha'} \to \Omega_{\alpha'}$:

$$\overline{H}_i(\xi) = \begin{cases} \dfrac{-1}{\mu}\left(\displaystyle\sum_{k \neq i}^{n} \omega_{ik} h(\xi_k) + \omega + z_i - \overline{x}_i\right) & \text{if } \alpha'_i = \text{“r”} \\ \dfrac{-1}{\mu + \omega}\left(\displaystyle\sum_{k \neq i}^{n} \omega_{ik} h(\xi_k) + z_i - \overline{x}_i\right) & \text{if } \alpha'_i = \text{“m”} \\ \dfrac{-1}{\mu}\left(\displaystyle\sum_{k \neq i}^{n} \omega_{ik} h(\xi_k) - \omega + z_i - \overline{x}_i\right) & \text{if } \alpha'_i = \text{“l”}\,, \end{cases}$$

where $\xi = (\xi_1, \ldots, \xi_n)$ and $\overline{H} = (\overline{H}_1, \ldots, \overline{H}_n)$. It is clear that $\overline{H}$ is a continuous function on $\Omega_{\alpha'}$. It follows from similar arguments as the proof of Theorem 3.4 that there exists a fixed point $\overline{\mathbf{x}}^{-1}$ of $\overline{H}$ and this point satisfies $F(\overline{\mathbf{x}}^{-1}) = \overline{\mathbf{x}}$.

(III) Let $\overline{\mathbf{x}}^{-1}$ be as obtained in (II). Similar arguments as in (II) confirm that there exists $\overline{\mathbf{x}}^{-2} \in \Omega_\alpha$ such that $F(\overline{\mathbf{x}}^{-2}) = \overline{\mathbf{x}}^{-1}$. Notably, $\overline{\mathbf{x}}^{-2}$ is chosen back into the region Ω_α containing $\overline{\mathbf{x}}$. Successively, we can find $\overline{\mathbf{x}}^{-l} \in \Omega_\alpha$ with $l \geq 3$. We compute the derivative DF of F on Ω_α as follows.

$$[DF]_{ik} = \begin{cases} \mu & \text{if } i = k, \alpha_k = \text{“l” or “r”}\,, \\ \mu + \omega & \text{if } i = k, \alpha_k = \text{“m”}\,, \\ 0 & \text{if } i \neq k, \alpha_k = \text{“l” or “r”}\,, \\ \omega_{ik} & \text{if } i \neq k, \alpha_k = \text{“m”}\,. \end{cases}$$

According to (PC-1-a), $\mu + \omega - \kappa_i > 1$ for all i. Thus, the absolute values of all eigenvalues of $DF(\mathbf{x})$ are larger than one for all $\mathbf{x}$, by the Gerschgorin's theorem. It follows that the absolute values of all eigenvalues of $DF^{-1}(\mathbf{x})$ are less than one, for all $\mathbf{x}$. Hence, F is expanding on Ω_α and F^{-1} is a contraction on $F(\Omega_\alpha)$, under certain norm on $\mathbb{R}^n$. Therefore, the sequence $\{\overline{\mathbf{x}}^{-l}\}$ lies on the unstable manifold of $\overline{\mathbf{x}}$ and $\overline{\mathbf{x}}^{-l} \to \overline{\mathbf{x}}$, as $l \to \infty$. We thus conclude that the fixed point $\overline{\mathbf{x}}$ is a snap-back repeller. The orbit $\{\overline{\mathbf{x}}^{-l}\}$ is exactly a homoclinic orbit. In fact, $\overline{\mathbf{x}}$ is the only fixed point (a snap-back repeller) in Ω_α, as F is expanding on Ω_α. ■

The construction in the proof of Theorem 3.5 shows that there are infinitely many different homoclinic orbits for a single snap-back repeller. For example, as we chose $\overline{\mathbf{x}}^{-2}$ in step (III), we could have chosen another pre-image of $\overline{\mathbf{x}}^{-1}$ under F, which lies in a region different from Ω_α. Indeed, there are at least 2^n possibilities to choose the pre-image of every point $\overline{\mathbf{x}}^{-l}$, $l \geq 2$, in the backward orbit $\{\overline{\mathbf{x}}^{-l} | l \in \mathbb{N}\}$ of $\overline{\mathbf{x}}$ under F.

3.3. *Numerical illustrations*

We plan to illustrate the dynamics of DT-CNN discussed in Secs. 2 and 3 by a two-cell DT-CNN. The parameters $\mu = 0.8$, $\omega = 0.3$, $\omega_{12} = \omega_{21} = 0.05$ and $z_1 = z_2 = 0$ satisfy Theorem 2.3. Thus DT-CNN with these parameters is completely stable. There are four attracting fixed points lying in $\Omega_{\star,*}$ with $\star, * =$ “l”, “r”, in Fig. 10.

Next, we illustrate the numerical ranges for the parameters satisfying condition (i) of Theorems 3.4 and 3.5. We use a Mathematica program to test whether if the inequalities in (PC-1) are satisfied for various parameters. Figures 11(a) and 11(b) give such an illustration. In Fig. 11(a), we locate the ranges for the parameters ω and κ satisfying (PC-1-a,-b,-c), with fixed $\mu = -1.8$. In Fig. 11(b), with $\kappa = 0$, the parameter ranges for μ and ω satisfying the condition (PC-1-a,-b,-c), are computed similarly.

Bifurcation diagrams for the iterations of x_1, x_2 with respect to the parameter ω as well as the Lyapunov exponents for DT-CNN with the parameters in the ranges in Figs. 11(a) and 11(b), are also demonstrated in Figs. 12(a)–12(c).

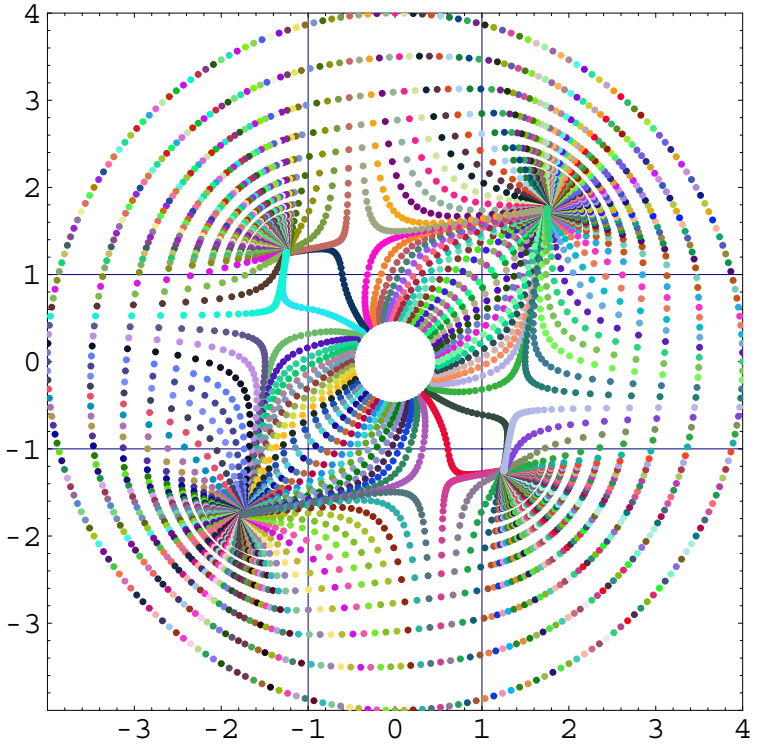

Fig. 10. Dynamics of DT-CNN on two dimensions with parameters $\mu = 0.8$, $\omega = 0.3$, $\omega_{12} = \omega_{21} = 0.05$ and $z = 0$. The initial values are chosen from two circles with center at the origin and radii 1/2 and 4, respectively. Every orbit in the figure approaches one of the four stable fixed points.

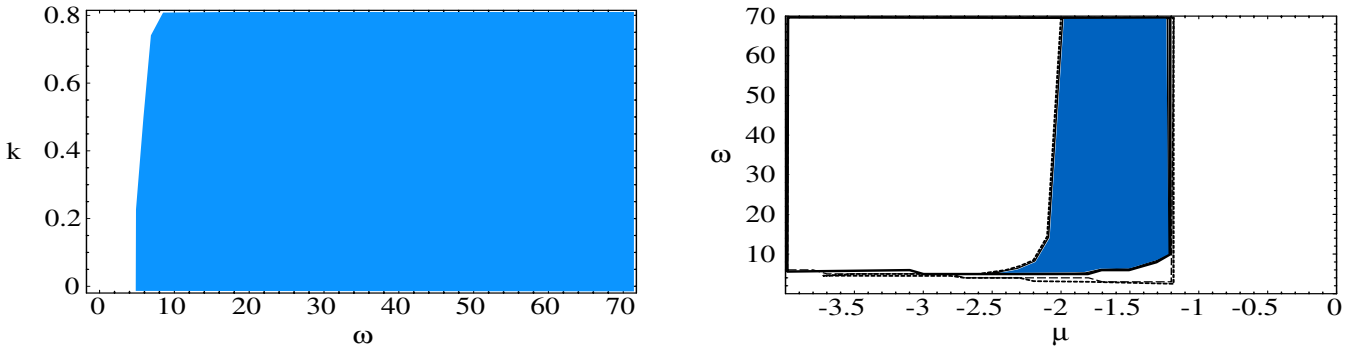

(a) (b)

Fig. 11. The parameter ranges for (a) (ω, k) with fixed $\mu = -1.8$, (b) (μ, ω) with fixed $k = 0$, which satisfy condition (PC-1-a,-b) of Theorems 3.4 and 3.5.

4. Local and Global Saturated Patterns of DT-CNN

A steady state (resp. pattern) $\overline{\mathbf{x}}$ (resp. $\overline{\mathbf{y}}$) of the cellular neural network is called saturated if every component of $\overline{\mathbf{x}}$ (resp. $\overline{\mathbf{y}}$) is either greater than one or less than minus one (resp. equal to one or minus one). A methodology of the formations of saturated patterns for CT-CNN has been developed by Juang and Lin [2000], and Shih [1998]. In this section, we shall illustrate that formations of saturated steady states and patterns for DT-CNN can be established exactly as in CT-CNN. Our treatments work for CT-CNN and DT-CNN of any dimension.

Let us take the DT-CNN with space-invariant template $[\alpha, a, \beta]$ on one-dimensional lattice for an

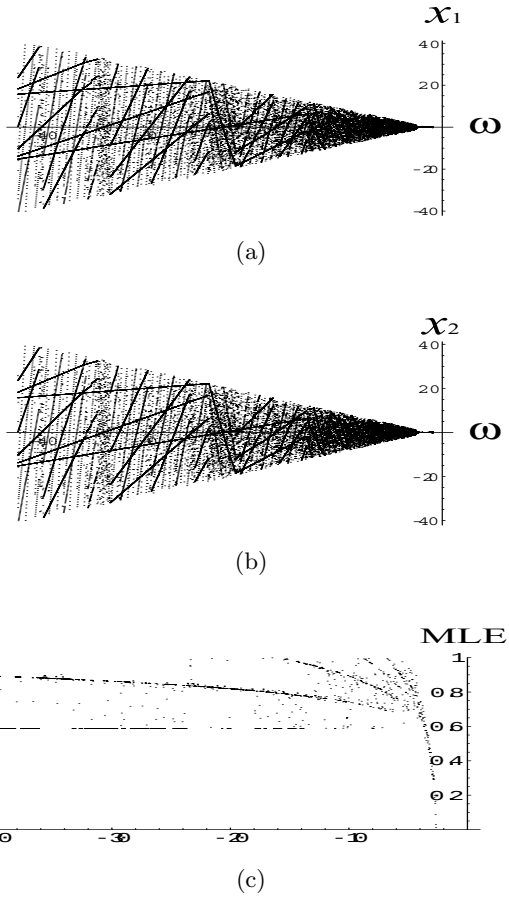

Fig. 12. The bifurcation diagram for (a) x_1, (b) x_2, with respect to the parameter ω. (c) Lyapunov exponent for various ω.

illustration. Consider, for $i \in T_m := \{k| -m \le k \le m\} \subset \mathbb{Z}$,

$$x_i(t+1) = \mu x_i(t) + \alpha h(x_{i-1}(t)) + a h(x_i(t)) + \beta h(x_{i+1}(t)) + z_i\,. \tag{30}$$

Usually, there are boundary conditions imposed on the two ends of the lattice T_m, cf. [Shih, 2000]. We omit this consideration for simplicity. The stationary equation for (30) is

$$-x_i + \tilde{\alpha} h(x_{i-1}) + \tilde{a} h(x_i) + \tilde{\beta} h(x_{i+1}) + \tilde{z}_i = 0\,, \tag{31}$$

where $\tilde{\alpha} = \alpha/(1-\mu)$, $\tilde{\beta} = \beta/(1-\mu)$, $\tilde{z}_i = z_i/(1-\mu)$ and $\tilde{a} = a/(1-\mu)$. For convenience of notations, we drop these "tilde".

If $a \neq 0$ and $\mathbf{x} = \{x_{-m}, \ldots, x_m\}$ is a solution of (31) with $|x_i| > 1$ for all $i \in T_m$ (that is, a saturated steady state solution of DT-CNN), then, for

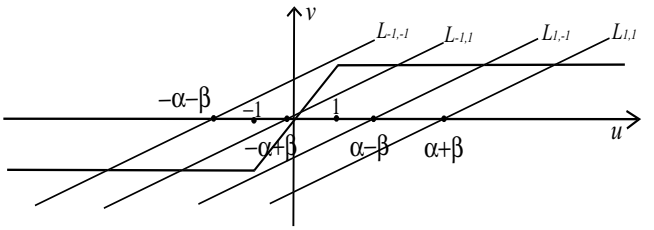

Fig. 13. $(\alpha, \beta) \in \Lambda_1$, $(z, a) \in [2; 1, 0]$. The four lines $L_{-1,-1}$, $L_{-1,1}$, $L_{1,-1}$, $L_{1,1}$ intersect u-axis at $-\alpha-\beta+z$, $-\alpha+\beta+z$, $\alpha-\beta+z$ and $\alpha+\beta+z$, respectively. (z is set to zero in the graph for simplicity.)

each $i \in T_m$, $(u, v) = (x_i, y_i = h(x_i))$ satisfies

$$\begin{cases} v = h(u) \\ v = \dfrac{1}{a}[u - (z_i + \sigma_1\alpha + \sigma_2\beta)] \end{cases} \tag{32}$$

for σ_1, $\sigma_2 = 1$ or -1. The expression in the second equation of (32) represents four straight lines on (u, v)-plane if a, α, $\beta \neq 0$, $\alpha \neq \pm\beta$, z_i are given. These four lines are labeled by $L_{\sigma_1\sigma_2}$, σ_1, $\sigma_2 = 1$ or -1 (see Fig. 13).

We first partition the (α, β)-plane so that the order of $\alpha+\beta$, $\alpha-\beta$, $-\alpha+\beta$, $-\alpha-\beta$ are fixed. For example, let $\Lambda_1 = \{(\alpha,\beta) \in \mathbb{R}^2 | \alpha+\beta > \alpha-\beta > -\alpha+\beta > -\alpha-\beta\}$. For $(\alpha,\beta) \in \Lambda_1$, then the four lines $\{L_{\sigma_1\sigma_2} | \sigma_1, \sigma_2 = \pm 1\}$ are positioned in order as in Fig. 13. Assume that the intersection of the four lines $L_{\sigma_1\sigma_2}$ with the graph of $v = h(u)$ is as Fig. 13. Consider

$$\begin{aligned}(y_{i-1}, y_i, y_{i+1}) &= (h(x_{i-1}), h(x_i), h(x_{i+1})) \\ &= (-1,1,1), (1,1,-1), (1,1,1), \\ &\quad (-1,-1,1), (-1,-1,-1)\,. \end{aligned} \tag{33}$$

Then (33) are the only 1×3 local saturated patterns for (30). Indeed, such scenario of intersection guarantees that there exist certain (x_{i-1}, x_i, x_{i+1}) satisfying (31), with their outputs as in (33). One can then attach these local solutions (patterns) to obtain the solutions (patterns) of (31) on T_m.

Thus, our second step is to partition the (z_i, a) parameter plane to classify the intersections of $\{L_{\sigma_1\sigma_2} | \sigma_1, \sigma_2 = \pm 1\}$ with the graph of $v = h(u)$. Fix i and set $(z, a) = (z_i, a)$. We take the example $(\alpha, \beta) \in \Lambda_1$ to explain the setting. Let us denote by "+" the output equals to one at a cell and "−" for the output equals to minus one at a cell. For $m, n = \{1, 2, 3\}$, we introduce the notation $[m; n] \subset (z, a)$-plane, which means that if $(z, a) \in [m; n]$, then the first $m+1$ lines (from the

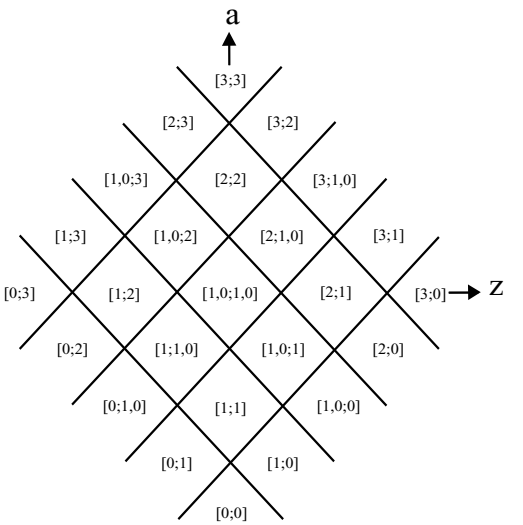

(a)

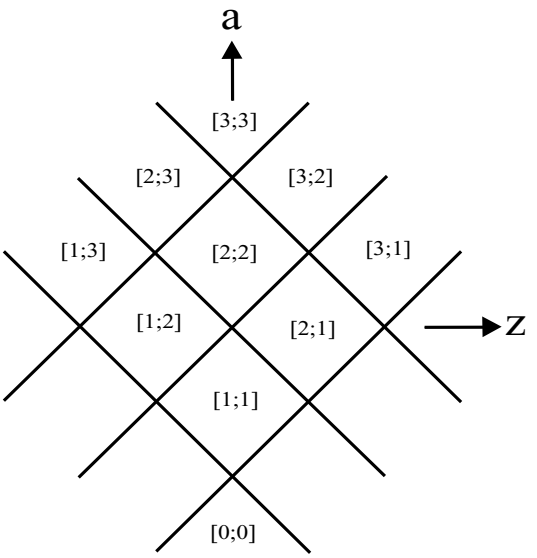

(b)

Fig. 14. (a) Partition of (z, a)-plane for given α, $\beta \neq 0$, $\alpha \neq \pm\beta$. (b) Partition of (z, a)-plane for given $\alpha \neq 0$, $\alpha = \beta$.

right) of $\{L_{\sigma_1\sigma_2} | \sigma_1, \sigma_2 = \pm 1\}$ intersect $v = h(u)$ at $u > 1$, and the first $n + 1$ lines (from the left) of $\{L_{\sigma_1\sigma_2} | \sigma_1, \sigma_2 = \pm 1\}$ intersect $v = h(u)$ at $u < -1$. Subsequently, (z, a) values can be classified into the following types.

(i) If $(z, a) \in [m; n]$, then the 1×3 local saturated patterns are exactly those with at least $(3-m)$ "+" (resp. at least $(3 - n)$ "−") in $\{w, e\}$ of $\underline{\overline{w + e}}$ (resp. in $\{w, e\}$ of $\underline{\overline{w - e}}$).

(ii) If $(z, a) \in [1, 0; 1, 0]$, then the 1×3 local saturated patterns are $\underline{\overline{w + e}}$, $\underline{\overline{w - e}}$ with $w =$ "+", $e =$ "+", "−".

(iii) if $(z, a) \in [1, 0; n]$, then the 1×3 local saturated patterns are $\underline{\overline{w - e}}$ with at least $3 - n$ "−" in $\{w, e\}$, and $\underline{\overline{w + e}}$ with $w =$ "−", $e =$ "+", "−".

(iv) If $(z, a) \in [m; 1, 0]$, then the 1×3 local saturated patterns are $\underline{\overline{w + e}}$ with at least $3 - m$ "+" in $\{w, e\}$, and $\underline{\overline{w - e}}$ with $w =$"−", $e =$ "+", "−".

For example, if $(\alpha, \beta) \in \Lambda_1$ and $(z, a) \in [2; 1, 0]$, then the 1×3 local saturated patterns are exactly the ones in the following form:

$$\underbrace{\underline{\overline{+++}}, \underline{\overline{++-}}, \underline{\overline{-++}}}_{\underline{\overline{w+e}}}, \quad \underbrace{\underline{\overline{---}}, \underline{\overline{--+}}}_{\underline{\overline{w-e}}}.$$

The partition of $(z, a) = (z_i, a)$-plane are illustrated in Figs. 14(a) and 14(b). Notably, in attaching local patterns into a pattern on T_m, one only needs to determine what 1×3 local saturated patterns are allowed at each site i. This process is not affected by the dependence of z_i on i.

References

Chen, S.-S. & Shih, C.-W. [2002] "Transversal homoclinic orbits in a transiently chaotic neural network," *Chaos* **12**, 654–671.

Chua, L. O. & Yang, L. [1988] "Cellular neural networks: Theory," *IEEE Trans. Circuits Syst.-I* **35**, 1257–1272.

Fiedler, B. & Gedeon, T. [1998] "A class of convergent neural network dynamics," *Physica* **D111**, 288–294.

Guckenheimer, J. & Holmes, P. [1983] *Nonlinear Oscillations, Dynamical Systems, and Bifurcations of Vector Fields*, Applied Mathematical Science, Vol. 42 (Springer-Verlag, NY).

Hale, J. & Raugel, G. [1992] "Convergence in gradient-like systems with applications to PDE," *ZAMP* **43**, 63–124.

Hänggi, M., Reddy, H. C. & Moschytz, G. S. [1999] "Unifying results in CNN theory using delta operator," *IEEE Int. Symp. Circuits Syst.* **3**, 547–550.

Harrer, H. & Nossek, J. A. [1992] "An analog implementation of discrete-time CNNs," *IEEE Trans. Neural Networks* **3**, 466–476.

Hsu, C.-H. & Lin, S.-S. [2000] "Existence and multiplicity of traveling waves in a lattice dynamical system," *J. Diff. Eq.* **164**, 431–450.

Juang, J. & Lin, S.-S. [2000] "Cellular neural networks: Mosaic patterns and spatial chaos," *SIAM J. Appl. Math.* **60**, 891–915.

LaSalle, J. P. [1976] *The Stability of Dynamical Systems*, Regional Conf. Series in Applied Mathematics, Vol. 25 (SIAM, Philadelphia).

Li, T. Y. & Yorke, J. A. [1975] "Period three implies chaos," *Amer. Math. Monthly* **82**, 985–992.

Lin, S.-S. & Shih, C.-W. [1999] "Complete stability for standard cellular neural network," *Int. J. Bifurcation and Chaos* **9**, 909–918.

Marotto, F. R. [1978] "Snap-back repellers imply chaos in $\mathbb{R}^n$," *J. Math. Anal. Appl.* **63**, 199–223.

Marotto, F. R. [1979] "Chaotic behavior in the Hénon mapping," *Commun. Math. Phys.* **68**, 187–194.

Sbitnev, V. I. & Chua, L. O. [2002] "Local activity for discrete-map CNN," *Int. J. Bifurcation and Chaos* **12**, 1227–1272.

Shih, C.-W. [1998] "Pattern formation and spatial chaos in cellular neural networks with asymmetric templates," *Int. J. Bifurcation and Chaos* **8**, 1907–1936.

Shih, C.-W. [2000] "Influence of boundary conditions on pattern formation and spatial chaos in lattice systems," *SIAM J. Appl. Math.* **61**, 335–368.

Shih, C.-W. & Weng, C.-W. [2000] "Cycle-symmetric matrices and convergent neural networks," *Physica* **D146**, 213–220.

Shih, C.-W. [2001] "Complete stability for a class of cellular neural networks," *Int. J. Bifurcation and Chaos* **11**, 169–177.

Shih, C.-W. & Weng, C.-W. [2002] "On the templates corresponding to cycle symmetric connectivity in cellular neural networks," *Int. J. Bifurcation and Chaos* **12**, 2957–2966.

This article has been cited by:

1. Xuemei Li, Zhaohui Yuan. 2009. Existence of periodic solutions and closed invariant curves in a class of discrete-time cellular neural networks. *Physica D: Nonlinear Phenomena* **238**:16, 1658-1667. [CrossRef]
2. Chih-Wen Shih, Jui-Pin Tseng. 2009. Global consensus for discrete-time competitive systems. *Chaos, Solitons & Fractals* **41**:1, 302-310. [CrossRef]
3. Xuemei Li. 2009. Analysis of Complete Stability for Discrete-Time Cellular Neural Networks with Piecewise Linear Output Functions. *Neural Computation* **21**:5, 1434-1458. [CrossRef]
4. Chen Feng-Juan, Li Ji-Bin. 2008. Metric horseshoes in discrete-time RTD-based cellular neural networks. *Neurocomputing* **71**:13-15, 2908-2913. [CrossRef]
5. FENG-JUAN CHEN, JI-BIN LI, FANG-YUE CHEN. 2008. HORSESHOE IN RTD-BASED CELLULAR NEURAL NETWORKS. *International Journal of Bifurcation and Chaos* **18**:03, 689-694. [Abstract] [References] [PDF] [PDF Plus]
6. XUYANG LOU, BAOTONG CUI. 2007. GLOBAL EXPONENTIAL STABILITY CONDITIONS FOR DELAYED PARABOLIC NEURAL NETWORKS WITH VARIABLE COEFFICIENTS. *International Journal of Bifurcation and Chaos* **17**:12, 4409-4415. [Abstract] [References] [PDF] [PDF Plus]
7. FENG-JUAN CHEN, JI-BIN LI, FANG-YUE CHEN. 2007. CHAOS FOR DISCRETE-TIME RTD-BASED CELLULAR NEURAL NETWORKS. *International Journal of Bifurcation and Chaos* **17**:12, 4395-4401. [Abstract] [References] [PDF] [PDF Plus]